

1 **The mid-8<sup>th</sup> century CE surface faulting along the Dead Sea Fault at Tiberias (Sea of Galilee, Israel)**

2  
3 **M. F. Ferrario<sup>1</sup>, O. Katz<sup>2</sup>, A. Hillman<sup>3</sup>, F. Livio<sup>1</sup>, R. Amit<sup>2</sup> and A. M. Michetti<sup>1</sup>**

4 <sup>1</sup> Università degli Studi dell'Insubria, via Valleggio 11, 22100 Como, Italy.

5 <sup>2</sup> Geological Survey of Israel, 30 Malkhe Israel Street, 95501 Jerusalem, Israel

6 <sup>3</sup> Israel Antiquities Authority.

7 Corresponding author: Maria Francesca Ferrario ([francesca.ferrario@uninsubria.it](mailto:francesca.ferrario@uninsubria.it))

8  
9 **Key Points:**

- 10 • Surface faulting affected the archaeological relics at the ancient Tiberias (Dead Sea Fault,  
11 Israel)
- 12 • We attribute this faulting to a mid-8<sup>th</sup> century CE earthquake
- 13 • Our findings highlight the need for revising the tectonic setting and seismic risk in the  
14 Sea of Galilee and nearby regions.

15 **Abstract**

16 The Dead Sea Fault (DSF) is a plate-boundary where large earthquakes are expected and largely  
17 overdue due to the lack of such events in the instrumental era. Sequences of earthquakes along  
18 the DSF are documented by historical evidence, one of the most devastating occurred in the mid-  
19 8<sup>th</sup> century CE. Here we describe site-specific archaeoseismological observations at the ancient  
20 Tiberias city, on the western shore of the Sea of Galilee. We map Roman and Byzantine relics  
21 faulted in the mid-8<sup>th</sup> century CE by a pure normal fault. We use geophysical, geomorphological  
22 and structural analyses integrated with published data, to assess the seismic hazard of the Jordan  
23 Valley Western Boundary Fault (JVWB). We propose that the normal JVWB can rupture the  
24 surface along its ~45 km trace running from Tiberias toward the S crossing Bet Shean, Tel  
25 Rehov and Tel Teomim. The JVWB, parallel to the main strike-slip Jordan Valley Fault  
26 segment, might be regarded as a major earthquake source in this region. We test the hypotheses  
27 of both single fault and multi-faults rupture scenarios, which result in an expected range of Mw  
28 from 6.9 (single rupture of the JVWB) to 7.6 (multiple rupture of the JVWB and Jordan Valley  
29 Fault). Our results suggest that seismic source characterization in the Sea of Galilee region must  
30 include normal faults capable of surface rupturing, despite the absence of such events in the  
31 instrumental catalogue.

32  
33 **KEYWORDS**

34 Dead Sea Fault; mid-8<sup>th</sup> century CE seismicity; Tiberias; archaeoseismology; seismic hazard;  
35 strain partitioning

36

## 37 **1 Introduction**

38 The spatial and temporal characterization of faults rupture, the expected magnitude range,  
39 fault dimension, focal mechanism and affected areas are primary parameters for the evaluation of  
40 the seismic hazard of a region. The time interval covered by reliable historical records is too  
41 short to have witnessed strong earthquakes, if these have recurrence intervals of hundreds of  
42 years. It is therefore vital to extend the time window covered by seismic catalogues, using  
43 archaeoseismological and paleoseismological evidence (e.g., Bozorgnia & Bertero, 2004;  
44 Michetti et al. 2005). However, a gross overestimation of the size of historical earthquakes can  
45 occur if many historical events occurred in quick succession are interpreted as a single  
46 earthquake (Ambraseys, 2005).

47 In this study we focus on the Sea of Galilee region (Israel), located along the Dead Sea  
48 Fault (DSF). The study area is particularly suitable for an archaeoseismological approach  
49 because it has a long human occupation and over 150 years of extensive archaeological  
50 excavations provide abundant relics pertaining to different historical periods. Strong earthquakes  
51 are known to have hit the Sea of Galilee area in historical times (e.g. Ambraseys, 2005, 2009;  
52 Guidoboni et al., 2007), whereas the instrumental catalogue is limited to  $M < 6$  earthquakes  
53 (recorded events since the first half of the 20<sup>th</sup> century). A seismic swarm (max  $M_w$  4.5)  
54 occurred in July-August 2018, with epicenters located in the NW part of the Sea of Galilee  
55 (Wetzler et al., 2019), renewing the interest in seismic risk evaluation in the area.

56 We document archaeoseismological evidence of normal surface faulting in the city of  
57 Tiberias, located on the W shores of the Sea of Galilee (Section 4.1), then we use  
58 morphotectonic data and newly acquired shallow geophysical prospection (Section 4.2) to  
59 characterize this normal fault. Based on our observations, we relate the damage of archaeological  
60 structures to the mid-8<sup>th</sup> century CE seismicity (Section 5.1) and discuss the structural setting and  
61 fault displacement hazard at Tiberias (Section 5.2) considering single and multi-fault rupturing  
62 scenarios (Section 5.3). Our data allow to: i) assess the kinematics and characteristics of the  
63 earthquake which generated the surface faulting at Tiberias during the mid-8<sup>th</sup> century CE, ii)  
64 define the trace and latest movement of an active fault crossing through the modern town of  
65 Tiberias and iii) highlight the need to consider several rupture scenarios for a comprehensive  
66 seismic risk assessment of the Sea of Galilee region.

## 67 **2 Study area**

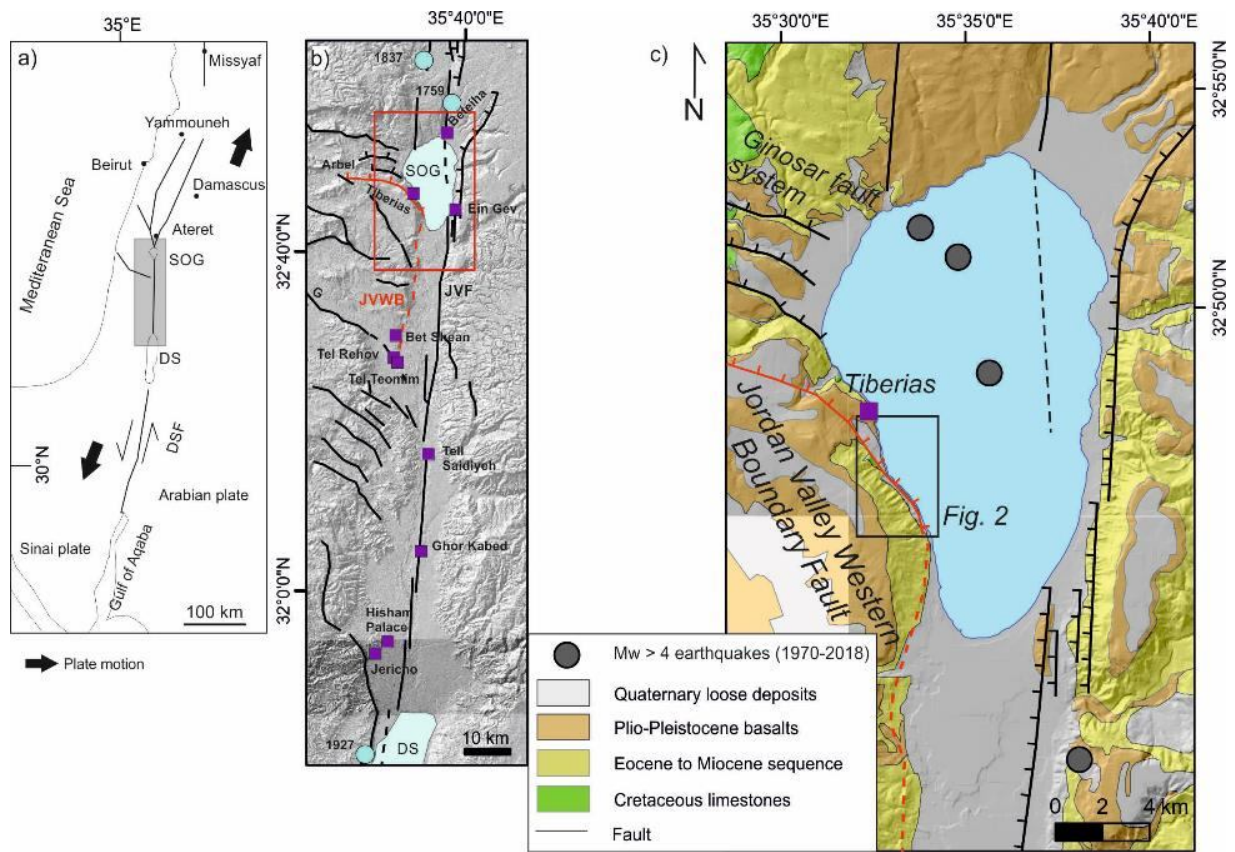
### 68 2.1 Structural and geologic setting

69 The DSF (Fig. 1a) forms the boundary between Arabia and Sinai plates and  
70 accommodates a long-term slip rate of about 4 – 5 mm/yr, resulting in 105 km of post-Miocene  
71 left-lateral displacement (e.g., Garfunkel, 1981; Garfunkel et al., 2014 and references therein). In  
72 the Sea of Galilee area, the main fault segment is the left-lateral Jordan Valley Fault (JVF),  
73 which runs along the E side of the Sea of Galilee (Marco et al., 2005; Hamiel et al., 2016;  
74 Wechsler et al., 2018 and reference therein; Fig. 1b). The JVF is characterized by Holocene left-  
75 lateral and normal components, which are estimated to be 4 - 5 mm/yr and 0.1 - 0.2 mm/yr  
76 respectively, based on paleoseismology (Ferry et al., 2007; Katz et al., 2010) and on GPS data.  
77 The latter indicates shallow creep behavior of the JVF along the SE coast of the Sea of Galilee  
78 (Hamiel et al., 2016).

79 The W coast of the Sea of Galilee is crosscut by a series of mostly E-dipping normal  
80 faults (Fig. 1c; Sneh, 2008; Sneh and Weinberger, 2014; Sagy et al., 2016; Sharon et al., 2020).  
81 North of Tiberias, these faults bend westward and assume an E-W trending (Fig. 1b, c).  
82 Southward a single fault is discontinuously traced until Tel Rehov and Tel Teomim, at the  
83 intersection with the Gilboa Fault (G in Fig. 1b). It is still debated whether the JVF and the  
84 normal faults at the W side of the Sea of Galilee presently accommodate the relative plate motion  
85 according to a strain-partitioned model (e.g., Garfunkel, 1981; Ben-Avraham & Zoback, 1992;  
86 Sagy et al., 2003), and thus might be regarded as individual seismic sources or, conversely, the  
87 Sea of Galilee is a pull-apart basin (e.g., Hurwitz et al., 2002) dissected on the western side by  
88 secondary normal faulting.

89 Previous studies investigated the W side of the Sea of Galilee at several sites through  
90 geological and geophysical research (Rotstein et al., 1992; ten Brink et al., 1999; Hurwitz et al.,  
91 2002; Sneh and Weinberger, 2014). The Hamat Tiberias hot springs (Fig. 2a) are interpreted as  
92 linked to a steep E-dipping normal fault (Ilani et al., 2006); geomorphic and structural evidence  
93 is used by Sagy et al. (2016; see also Garfunkel et al., 1981) to map a series of active and  
94 potentially active normal fault segments for a total length of 40 - 45 km up to Tel Rehov and Tel  
95 Teomim, where Late Pleistocene normal faulting has been described in detail, also through  
96 exploratory trenching (Garfunkel et al., 1981; Zilbermann et al., 2004; Sagy et al., 2016). Field  
97 mapping, offset landforms and exploratory excavations allow to estimate the Quaternary normal  
98 slip rate of this fault in 0.5 – 2 mm/yr, without significant strike-slip component (Hurwitz et al.,  
99 2002; Zilbermann et al., 2004; Eppelbaum et al., 2004, 2007). In the following, we refer to the  
100 whole segment from Arbel to Tel Rehov and Tel Teomim as the Jordan Valley Western  
101 Boundary Fault (JVWB), and for modelling purposes we assume that it is continuous at the sub-  
102 surface (Fig. 1b).

103 The stratigraphic setting of the W side of the Sea of Galilee (Fig. 1c) is characterized by a  
104 Plio-Pleistocene basaltic plateau which overlies Cretaceous limestones and Neogene-Quaternary  
105 basin infillings. Well-developed triangular facets and wineglass-shaped valley outlets, fluvial  
106 elbows and river captures suggest a tectonic origin for the range front residing along the W side  
107 of the Sea of Galilee (Fig. 2).



108

109 **Figure 1.** Structural framework of the Tiberias area; a) plate tectonic setting of the Dead  
 110 Sea Fault (DSF), the grey box locates the area shown in (b), between the Sea of Galilee (SOG)  
 111 and the Dead Sea (DS); b) Quaternary faults in the central part of the DSF, modified after Sneh  
 112 and Weinberger (2014), Sagy et al. (2016), Hamiel et al. (2016) and Sharon et al. (2018, 2020);  
 113 the red rectangle is the area enlarged in c); JVWB: Jordan Valley Western Boundary Fault,  
 114 JVF: Jordan Valley Fault, G: Gilboa Fault; c) simplified geologic map (after Bogoch & Sneh,  
 115 2008; Sneh, 2008), epicenters of  $M_w > 4.0$  events since 1970 (data from  
 116 <http://seis.gii.co.il/en/earthquake/searchEQSRslt.php>).

117

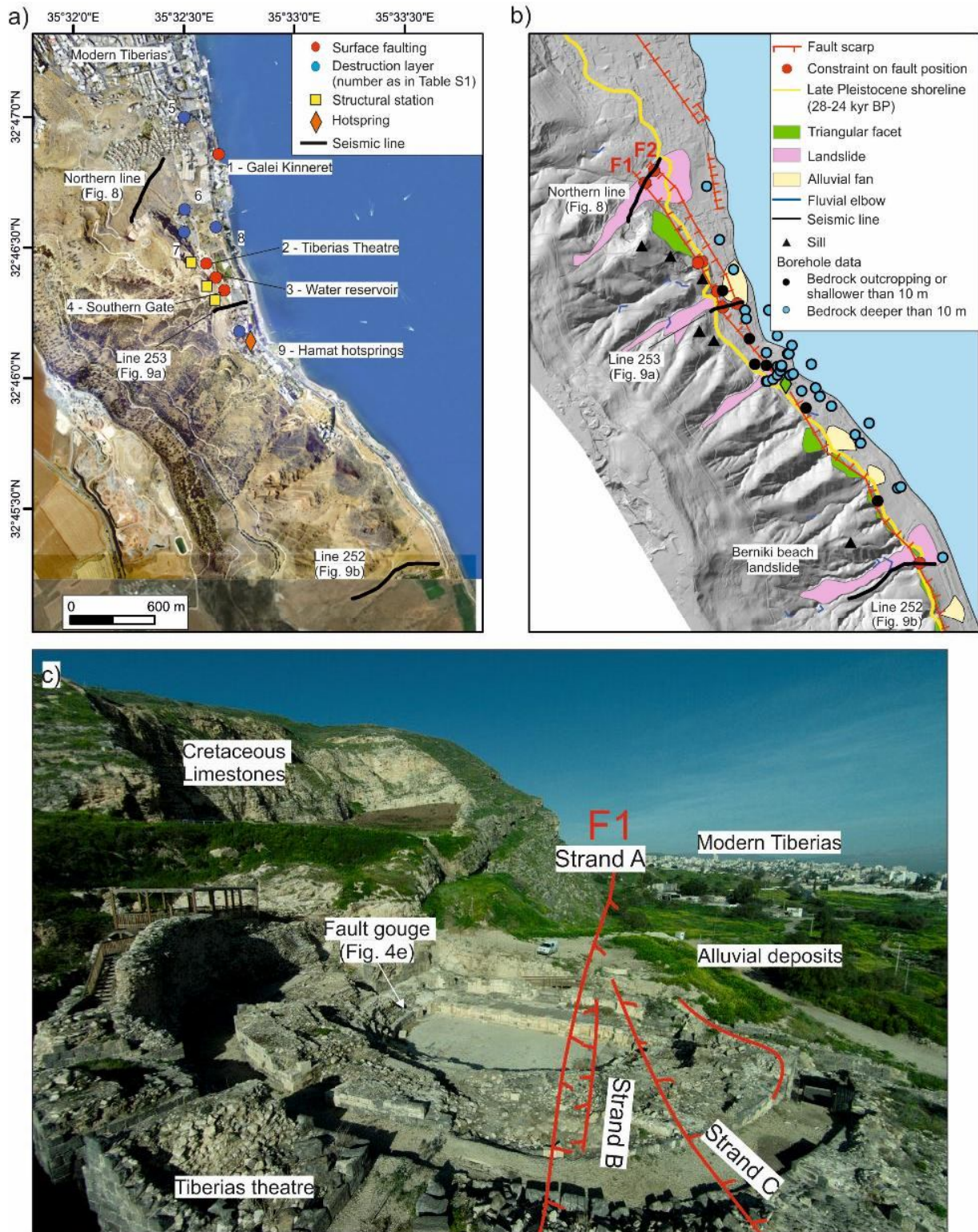
## 118 2.2 Historical evolution and investigated sites at Tiberias

119 The Roman city of Tiberias was founded in the name of Emperor Tiberius by Herod  
 120 Antipas in 19 CE. Archaeological excavations carried out at Tiberias reported abundant  
 121 earthquake-related damage in archeological strata (Hirschfeld & Meir, 2004; Hirschfeld &  
 122 Gutfeld, 2008; Zingboym & Hartal, 2011; Dalali-Amos, 2016; Onn & Weksler-Bdolah, 2016).  
 123 We performed our investigations at three sites (namely the Theatre, the Southern Gate and a  
 124 water reservoir), near the southern part of the modern city (Fig. 2a).

125 Atrash (2010) reconstructed several building phases in the studied Theatre (Fig. 3a):  
 126 during the earliest building phase (Stratum V, 1<sup>st</sup> century CE), the Theatre had two blocks of  
 127 seats; in the second phase (Stratum IV, 2<sup>nd</sup>-3<sup>rd</sup> century CE) a third block of seats and a larger  
 128 *auditorium* were added. In the third phase (Stratum III, 4<sup>th</sup>-6<sup>th</sup> century CE), the third block of

129 seats was dismantled and a tribune was added. In the Late Byzantine to Umayyad period, the  
130 Theatre has been downscaled and then abandoned, as testified by debris flow deposits that buried  
131 the site. Finally, a Fatimid-Abassid residential quarter (Strata I-II, 8<sup>th</sup>-11<sup>th</sup> century CE) was built  
132 on the Theatre remains and was in use until late 11<sup>th</sup> century CE (Atrash, 2010). The Fatimid-  
133 Abassid structures were completely removed during the excavation in 2009.

134         The Southern Gate, located ca. 200 m S of the Theatre (Fig. 2a), was originally built  
135 during the Early Roman period as a free-standing structure. In Byzantine times, the gate was  
136 incorporated in the city wall and in Umayyad-to-Fatimid periods other buildings and retaining  
137 walls were constructed at the site (Hartal et al., 2010). Between the Theatre and Southern Gate,  
138 an Umayyad water reservoir was uncovered in 2017.



139

140

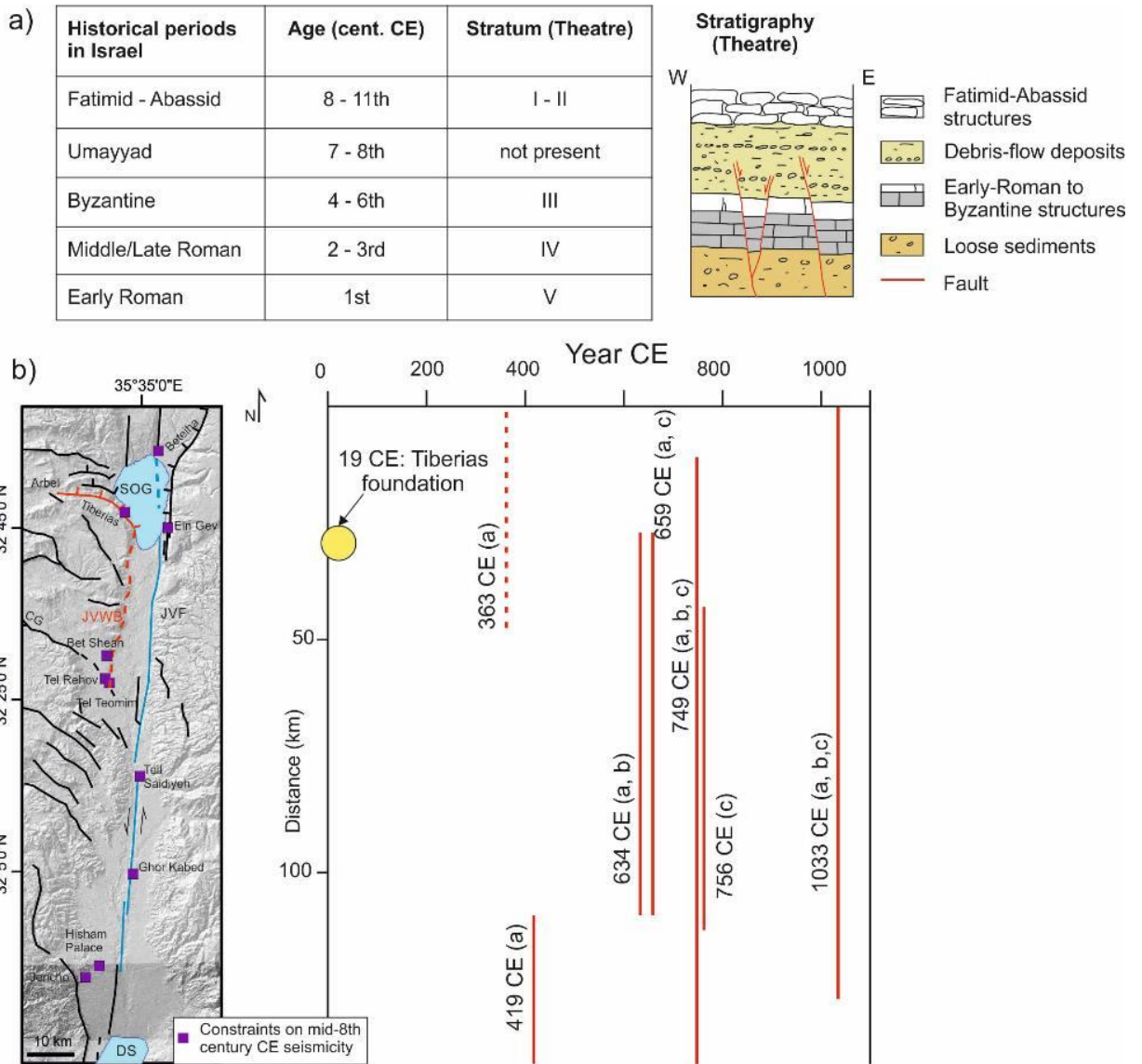
141

142

**Figure 2.** a) Relevant sites mentioned in the text and location of the seismic lines; numbers correspond to Table S1 where relevant references are provided; b) Morphotectonic map of the study area, based on 0.5-m resolution DTM extracted from airborne Lidar survey.

143 The map shows also the late-Pleistocene shoreline, the position of boreholes analyzed in this  
 144 study and the points where we constrained the spatial position of the fault trace. c) Drone  
 145 picture of Tiberias Theatre (foreground), the outcropping limestone and the modern town  
 146 (background), photo courtesy of Y. Darvasi.

147



148

149 **Figure 3.** a) Historical periods in Israel and schematic stratigraphic column at the  
 150 Theatre; b) Map of Quaternary faults, the JFWB and JVF are highlighted in red and blue,  
 151 respectively; spatial and temporal distribution of the major documented earthquakes (estimated  
 152 magnitude above ca. 6) that affected the Jordan Valley between Tiberias foundation at 1<sup>st</sup>  
 153 century CE and the 11<sup>th</sup> century CE. Data are from published literature, indicated by the letters  
 154 in brackets; a: Agnon (2014), b: Marco & Klinger (2014) and c: Zohar (2019). Vertical bars  
 155 represent the presumed spatial extent of ruptures relative to the faults map; the 363 CE event is  
 156 shown as a dashed line because it is not attributed to the JVF.

157

## 158 2.3 Historical seismicity: constraints from literary sources and geological investigations

159 Information on past earthquakes along the DSF is particularly rich and includes evidence  
160 for strong but infrequent earthquakes derived from historical, archaeological and geological data  
161 (Guidoboni et al., 2007; Ambraseys, 2009; Agnon, 2014; Zohar et al., 2016). Here we limit our  
162 description to the region between the Sea of Galilee and the Dead Sea. For a thorough review of  
163 the historical seismicity along the entire DSF and related paleo- and archaeoseismological  
164 evidence, the reader is referred to the several review papers published on this topic (e.g.,  
165 Guidoboni et al., 2007; Ambraseys, 2009; Agnon, 2014; Garfunkel et al., 2014; Marco &  
166 Klinger, 2014; Zohar et al., 2016; Zohar, 2019). An integration of data from recent seismology,  
167 historical, archeological and paleoseismological investigations revealed that the recurrence  
168 interval in Sea of Galilee region is about 500 and 1500 years for earthquakes of  $M_w > 6$  and  $M_w$   
169  $> 6.5$ , respectively (Ambraseys, 2009; Hamiel et al., 2009; Katz et al., 2010). Such large  
170 earthquakes may generate ground acceleration up to 0.5g and earthquake-induced landslides  
171 around the Sea of Galilee (Katz et al., 2010).

172 Fig. 3b summarizes the earthquakes that occurred in the studied region since Tiberias  
173 foundation (1<sup>st</sup> century CE) and the 11<sup>th</sup> century CE. In the following, we provide more details  
174 on the mid-8<sup>th</sup> century CE seismicity, the most relevant for our study. During this period, a  
175 sequence of strong earthquakes spatially and temporarily clustered occurred along the DSF. They  
176 were felt over a large area extending between N Syria and Egypt, but the amalgamation of  
177 literary information (e.g., Karcz, 2004; Ambraseys, 2005, 2009) resulted in an unlikely image of  
178 damaging produced by a single event (i.e., estimated  $M_w$  7.0-7.5; Marco et al., 2003).  
179 Theophanes, a reliable and almost contemporary source, mentions three distinct earthquakes  
180 between 747 and 757 CE (Ambraseys, 2005). The precise dating of the events is debated,  
181 although numismatic indications constrain destruction at Bet Shean (Scythopolis), located along  
182 the southern part of the JWVB (Fig. 3b), after August 748 CE (Tsafirir & Foerster, 1992; Karcz,  
183 2004).

184 Several authors dealt with the mid-8<sup>th</sup> century CE seismicity, based on archaeological,  
185 paleoseismic and macroseismic studies. Starting from the N, paleoseismic evidence matching  
186 this time frame was found along the Missyaf (Meghraoui et al., 2003) and Yammouneh (Daeron  
187 et al., 2007) Faults (Fig. 1a). At Galei Kinneret, about 1.5 km N of the Theatre (Fig. 2a), Marco  
188 et al. (2003) documented secondary E-dipping normal faults affecting archaeological ruins dated  
189 as late as the early 8<sup>th</sup> century CE, whereas buildings from the late 8<sup>th</sup> century CE were not  
190 faulted. Along the JVF (Fig. 1b), paleoseismic surface ruptures related to the same event were  
191 found at Beteiha (Wechsler et al., 2018), Ein Gev (Katz et al., 2010), Tell Saidiyeh and Ghor  
192 Kabed (Ferry et al., 2007). At Hisham Palace (Jericho), Reches & Hoexter (1981) documented  
193 surface faulting as well. Damage at this site has been re-assessed as due to the 1033 CE  
194 earthquake (Alfonsi et al., 2013), but the latter study did not address the main fault strand, thus a  
195 mid-8<sup>th</sup> century event cannot be definitely excluded. South of the Dead Sea, a rupture matching  
196 the mid-8<sup>th</sup> century CE interval and extending to the Gulf of Aqaba (Fig. 1a) is inferred by  
197 Agnon (2014) using macroseismic and archaeological evidence, and by Lefevre et al. (2018)  
198 using paleoseismological investigations.

199 More recently, the Sea of Galilee region was hit by several strong earthquakes, including  
200 the 1759 (two events with  $M_s$  6.6 and 7.4; Ambraseys & Barazangi, 1989) and the 1837 ( $M_s$  7.1;

201 intensity VIII MSK at Tiberias according to Ambraseys, 1997; and IX MM according to Vered  
202 & Striem, 1977). In 1927, a Ml 6.25 earthquake occurred near Jericho (see Fig. 1b for position;  
203 Ben-Menahem et al., 1976), with epicentral intensity of IX MSK (Avni et al., 2002).

## 204 2.4 Instrumental seismicity

205 The instrumental catalogue (<http://seis.gii.co.il/en/earthquake/searchEQS.php>) includes  
206 77 earthquakes with  $M_w > 2.5$  in the area depicted in Fig. 1c since 1970, 4 of which had  $M_w >$   
207 4.0. These include a  $M_w$  4.0 occurred in 2011 along the JVF and 3 events with epicenter  
208 offshore in the Sea of Galilee (Fig. 1c). The oldest one in the catalogue ( $M_w$  4.2) occurred in  
209 1972, whereas the 2 most recent ( $M_w$  4.5 and 4.2) occurred in July 2018 as part of a swarm of  
210 shallow earthquakes with normal focal mechanism solutions (focal depth  $< 10$  km). Seismicity is  
211 located offshore, in the NW part of the Sea of Galilee, aligned along NNW-SSE direction  
212 (Wetzler et al., 2019).

## 213 3 Materials and methods

### 214 3.1 Morphotectonics

215 We use high resolution airborne-Lidar based topographical model, acquired for the entire  
216 Sea of Galilee coastal area by Ofek Aerial Photo, using Optech ORION H300 (covered area:  
217 over 150 km<sup>2</sup>). Products include ground-validated DSM and DTM with pixel size of 0.5 m x 0.5  
218 m and average vertical error of less than 10 cm. We process the data obtaining maps of slope,  
219 aspect and contour lines. We interpret multiscale aerial photos (two coverages imaging the area  
220 at 1945 and 1982) using an analogic stereoscope.

221 We map linear and areal features with a clear geomorphic expression at the surface (i.e.,  
222 abrupt change in topography and slope) and discriminate tectonic from lacustrine features (e.g.,  
223 late Pleistocene shorelines; Hazan et al., 2005) and man-made structures using Lidar data and  
224 high spatial resolution satellite images (Esri imagery). We check available borehole logs and  
225 cores available at the Geological Survey of Israel archives, providing additional data on the  
226 shallow subsurface. We implement information in a GIS database and finally we directly study  
227 the mapped elements through field reconnaissance. We draw geologic cross-sections at three key  
228 sites, using surface (fieldwork, Lidar and aerial imagery interpretation) and shallow subsurface  
229 (seismic lines and borehole logs) constraints.

230 We consider the mapped faults as highly reliable due to at least one of the following  
231 reasons: (i) were directly observed at the archaeological sites, (ii) investigated through seismic  
232 lines, (iii) deduced from borehole logs, (iv) mapped in the official Israeli active fault map (Sagy  
233 et al., 2016), (v) described in detail in scientific literature (e.g., Marco et al., 2003).

### 234 3.2 Archaeoseismology and structural analysis

235 We surveyed Tiberias Theatre and the Southern Gate in 2014-2015. Archaeological  
236 stratigraphy (Atrash, 2010; Hartal et al., 2010) enabled to date the relics and related damage. We  
237 acquire about 30 high-resolution low-aerial photographs from different perspectives and heights  
238 using a DJI Phantom drone.

239 We classify Earthquake Archaeological Effects (EAE) according to type (fractures on  
240 ground or on walls, folded walls, chip corners), following the guidelines provided by Rodriguez-

241 Pascua et al. (2011). Damage was mapped on a high-resolution image acquired by a UAV-  
242 airborne camera. We measure structural data (dip direction and dip) on 182 fractures within the  
243 archaeological sites (see Table S2) using a compass or an Android mobile equipped with  
244 FieldMove CLINO app by Petroleum Experts Limited®, and we plot data using Stereonet v.11  
245 software by Rick Allmendinger  
246 (<http://www.geo.cornell.edu/geology/faculty/RWA/programs/stereonet.html>). We measure a set  
247 of 15 fault planes with kinematic indicators on the outcropping bedrock at 3 different stations  
248 between the Theatre and the Gate (raw data are listed in Table S3). We invert for slip with the  
249 software FaultKin v.8 (Allmendinger et al., 2001), following a kinematic approach (i.e.,  
250 Unweighted Moment Tensor Solution) in order to derive strain axes from fault geometry and slip  
251 direction. This method assumes that slip direction on fault is parallel to the maximum resolved  
252 shear rate of a large-scale homogeneous strain rate tensor (e.g., Marrett & Allmendinger, 1990).

253 We carry out high resolution topographic surveys using a total station (Sokkia; SET3R),  
254 focused on seat courses and wall stones, considered as an originally horizontal datum, in order to  
255 measure vertical displacement with cm-scale accuracy. We carefully selected the location of the  
256 profiles, to target original elements, not replaced during the restoration process.

### 257 3.3 Seismic survey

258 For the purpose of this study three high resolution seismic reflection profiles were  
259 acquired by the Geophysical Institute of Israel to image the shallow subsurface of the faults  
260 recognized at Tiberias Theatre and the Southern Gate (see Section 4.2). Lines were placed in  
261 order to intercept morphologic lineaments interpreted as possibly connected to active tectonics.

262 The first two lines are located close to the Southern Gate (Line 253) and at Berniki Beach  
263 landslide (Line 252), i.e., 2.5 km S of Tiberias Theatre (Fig. 2a). The following parameters are  
264 used: 500 mSec record length, 0.5 mSec sample rate, 2.5 or 5 m shot intervals using 48 channels  
265 (Medvedev, 2008). The energy source is a Digipulse and the recorder is a Strata View RX-60.  
266 For the third line, located N of Tiberias Theatre (Northern Line; Fig. 2), high density data are  
267 collected using a 2 Sec record length and 1 mSec sample rate. The line included 201 channels in  
268 2.5 m intervals. A reflection survey with a tomography approach has also been conducted. The  
269 data is recorded using a Geometrics Geode system and Oyo Geospace GS-32CT 10 Hz  
270 Geophones. The seismic source wavelet is generated by a M27 HR truck mounted vibroseis.  
271 Data are processed using the Landmark® (ProMax) software; optimal signal/noise ratio is  
272 obtained through noise attenuation and band-pass filtering. Data visualization and interpretation  
273 is realized using SeiSee software, and is based on reflectors dip and continuity, whereas lines  
274 were drawn through commercial graphic software. Further details on the processing steps are  
275 provided in Text S1.

## 276 4 Results

### 277 4.1 Archaeoseismological observations

#### 278 4.1.1 Evidence for surface faulting: the Tiberias Theatre and the Southern Gate

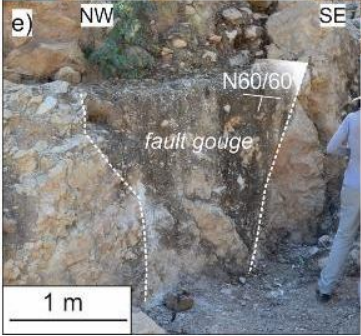
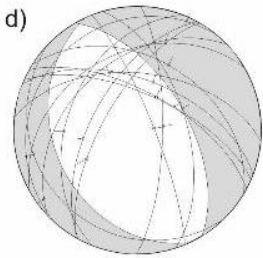
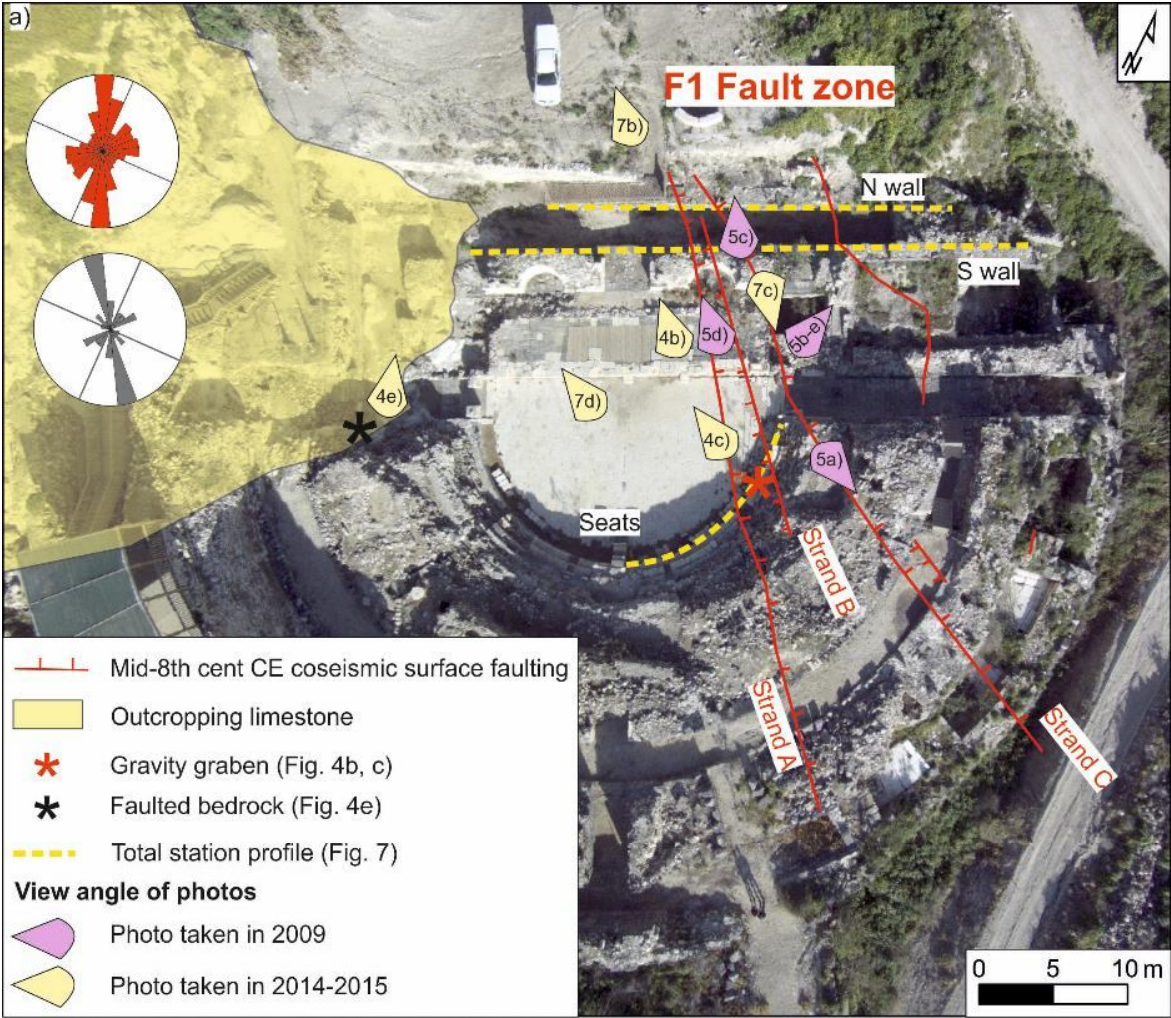
279 We performed original surveys in 2014-2015; the present-day status of the site is shown  
280 in Fig. 4, together with the view angle of photos; Fig. 5 shows pictures taken at the Theatre

281 during the 2009 excavations and Fig. 6 shows data on the Southern Gate and water reservoir;  
282 clean images are provided in the supplementary material (Fig. S2-S13).

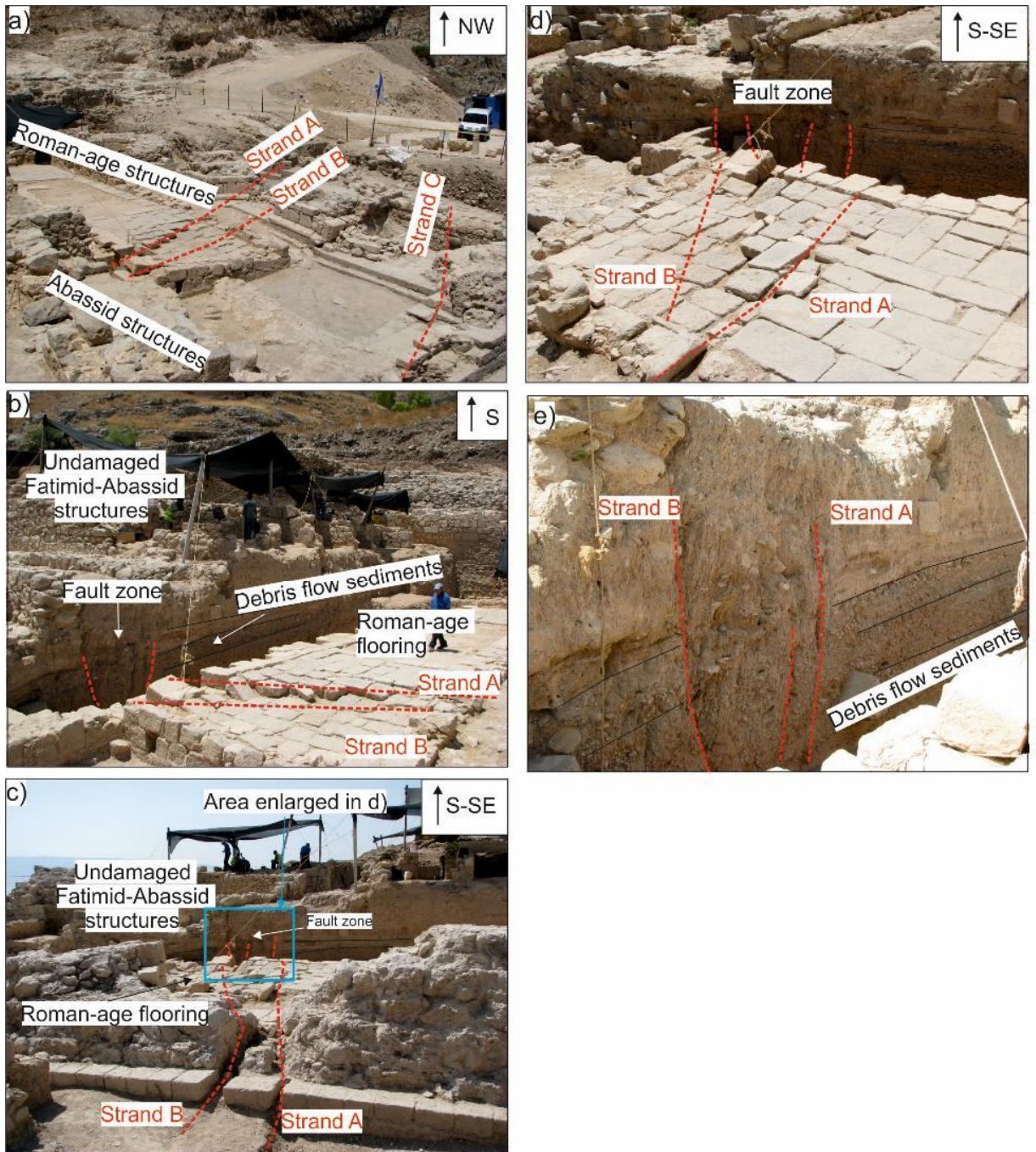
283 Cretaceous limestones outcrop in the NW side of the Theatre (Fig. 4a), while the E side  
284 lies on loose alluvial deposits (see Fig. 2c for an aerial view). Close to this contact, a bedrock  
285 fault zone (N060/60) is exposed as a 1.5 m thick fault gouge (Fig. 4e). Stress inversion of fault  
286 slip data, collected at three structural station between the Theater and the Gate (Fig. 4d and Table  
287 S3; location of structural stations is shown in Fig. 2a) indicates an almost pure extensional  
288 regime, with a T axis trending N062/13. The limestone – alluvial deposit contact has a clear  
289 morphological expression out of the Theatre area (i.e., lies at the base of the mountain  
290 escarpment) and is interpreted as tectonic in origin on the Israeli map of active faults (Sagy et al.,  
291 2016).

292 The Theatre preserves evidence of deformation (Fig. 4a), mainly aligned along a ca. 10 m  
293 wide, N140-trending, belt which is located ca. 30 m to the E of the bedrock fault gouge described  
294 above. These archaeoseismic effects include on-fault effects with vertical displacement  
295 (downthrown seat-rows and walls) and strain structures generated by permanent ground  
296 deformation (tilted and folded walls). All these features belong to the primary earthquake  
297 archaeological effects described by Marco (2008) and Rodriguez-Pascua et al. (2011). The most  
298 relevant feature is a 5-m wide, at least 15 m long, coseismic gravity-graben affecting the  
299 orchestra limestone pavement and lower block of seats (Fig. 4b-c). High resolution topographic  
300 surveys carried out along several transects on features considered as a horizontal datum (i.e.,  
301 flagstones and seat rows), show 50-to-60 cm of vertical net throw with downthrown side to the E  
302 (Fig. 7a-d), including both discrete and distributed deformation.

303 Photos taken in 2009 during the archaeological excavation show that normal  
304 displacement affects Roman-age floorings as well as debris flow sediments covering the Theatre  
305 pavement (Fig. 5). The sediments are well-bedded for their entire exposure, except for a few  
306 meters wide zone, corresponding with the fault zone.



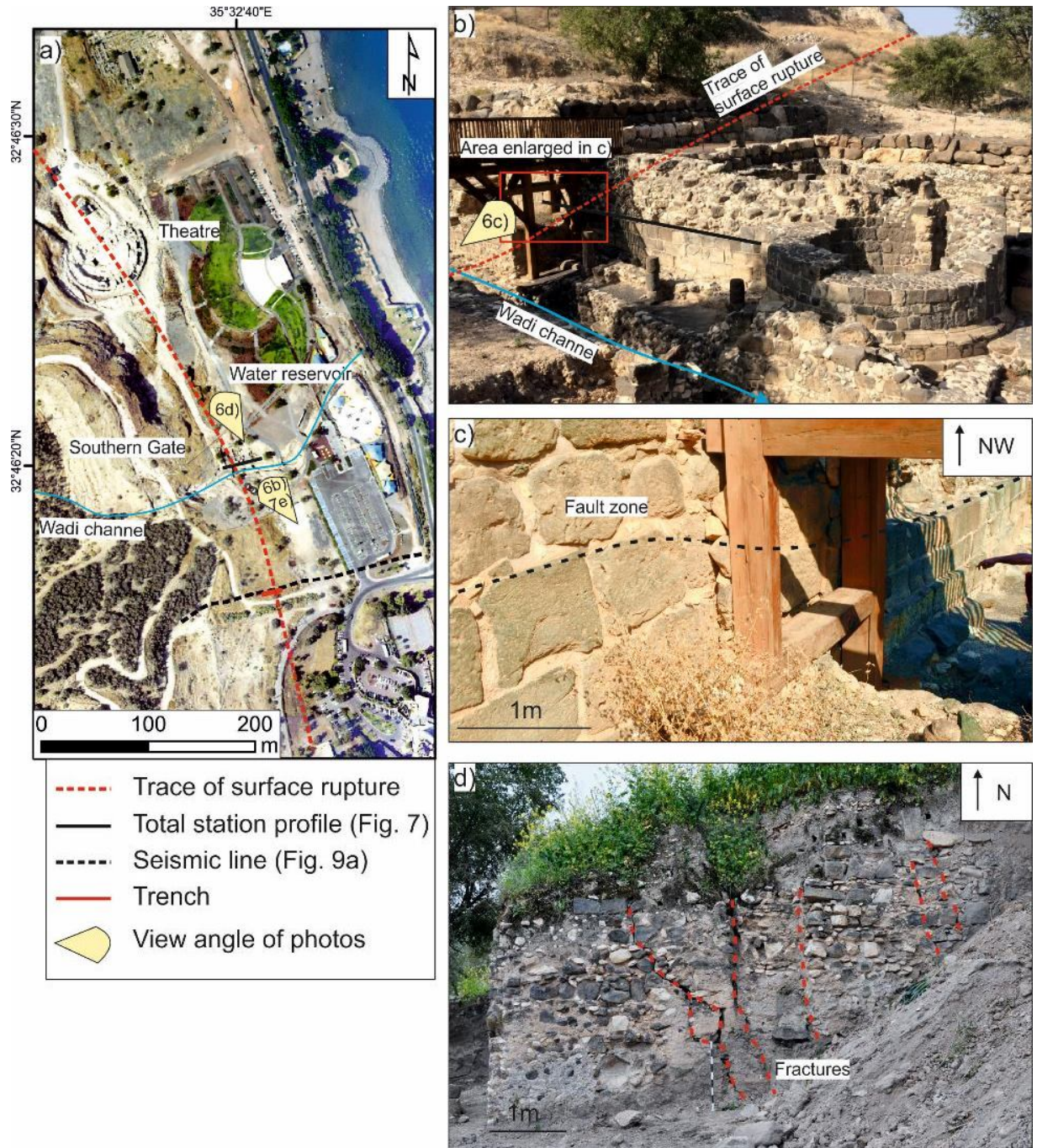
308 **Figure 4.** Surface faulting at the Tiberias Theatre: a) map of ruptures across the Theatre,  
 309 rose diagrams (bin size 15°) plot the strike of mode I fractures on building stones from the whole  
 310 site (red,  $n^\circ 100$ ) and on the orchestra floor (grey,  $n^\circ 23$ ); picture view angles (the figure number  
 311 showing each picture is indicated) and trace of total station profiles are shown as well; b-c)  
 312 details of the gravity graben displacing seat rows and walls; d) right dihedral best fit solution of  
 313 fault slip inversion (15 fault planes in the limestone bedrock, surveyed between the Theater and  
 314 the Gate; Table S3); e) detail of the limestone normal fault gouge (site is shown in a).  
 315



317 **Figure 5.** *Interpreted photographs taken during excavations at Tiberias Theatre in 2009*  
318 *(photo courtesy of S. Marco). a) panoramic view on damaged Roman-age structures (fault trace*  
319 *is marked by red dashed line) overlaid by Fatimid-Abassid undamaged structures; b) damaged*  
320 *Roman Theatre flooring overlaid by faulted alluvial sediments (fault trace is marked by red*  
321 *dashed line) and undamaged Fatimid-Abassid structures; c) damaged Roman Theatre wall,*  
322 *overlaid by faulted alluvial sediments; d) detail of the damaged Roman flooring and the faulted*  
323 *alluvial sediments; e) detail on the faulted debris flow sediments..*

324

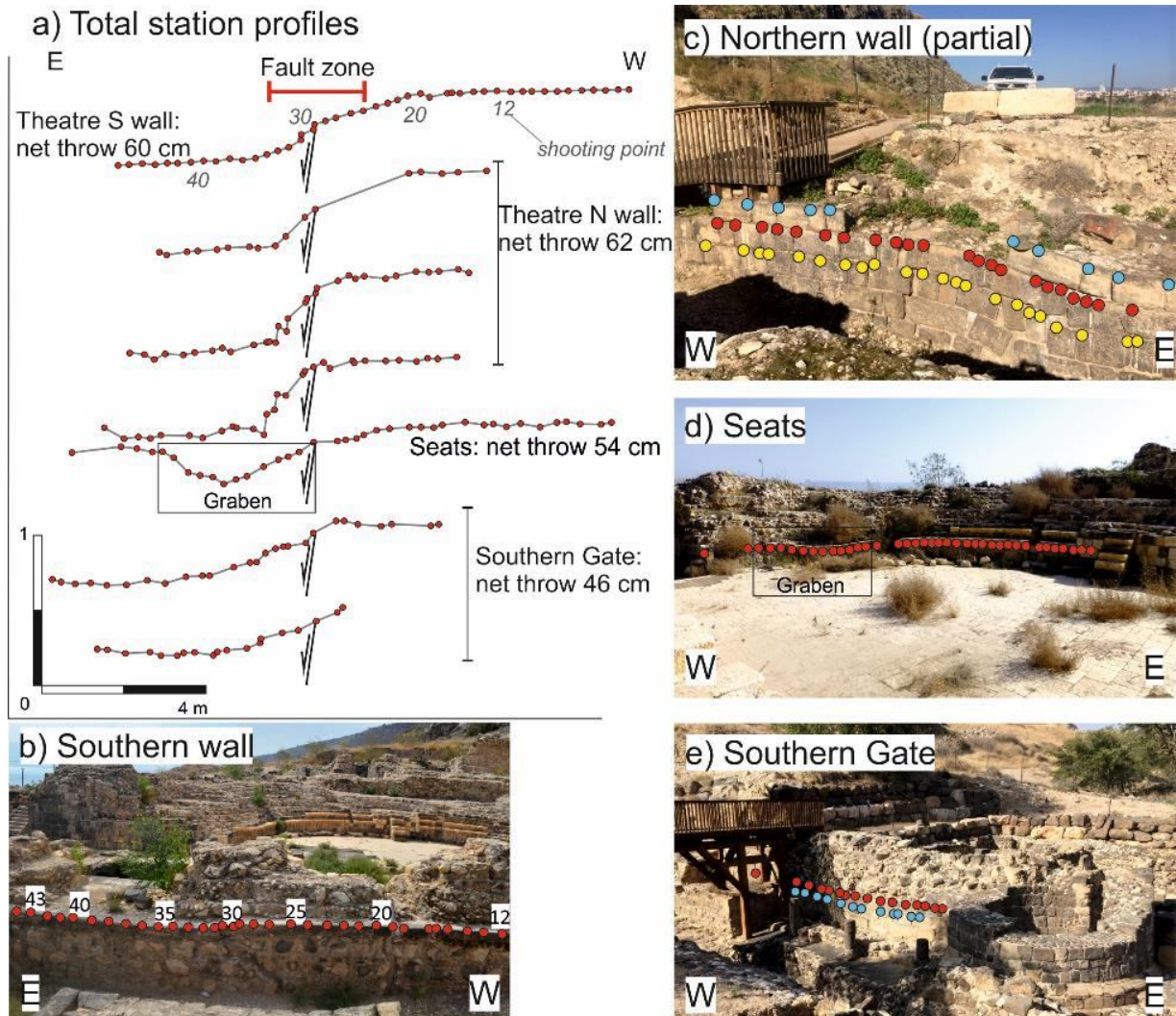
325 The Southern Gate is built on a bedrock (Cretaceous limestone), which outcrops at the  
326 base of the wadi channel running in a general E-W direction within the site. Displacement at the  
327 Southern Gate is represented by warping of a Byzantine E-W wall, archaeologically dated at ca.  
328 530 CE (Fig. 6b-c). A total station profile shows ca. 45 cm of total throw with downthrown side  
329 to the E (Fig. 7a, 7e). The measured displacement has a pure normal component with an amount  
330 of vertical displacement similar to that recorded at the Theatre.



331

332 **Figure 6.** a) Map of the Southern Gate and water reservoir sites, ca. 200 m S of the  
 333 Theatre, along the JVWB Fault strike, with indication of picture view angles, trace of total  
 334 station profile, seismic Line 253 and exploratory trench. Fault trace is marked by red dashed  
 335 line; b) view of the Byzantine wall at the Southern Gate site; c) detail of the warped Byzantine  
 336 wall. The wooded frame, holding the pedestrian bridge, is situated above the fault line. The  
 337 dashed black line marks a down throw of an originally horizontal datum; d) set of fractures  
 338 affecting the Umayyad water reservoir located in between the Theatre and the Southern Gate.

339



340  
 341 **Figure 7.** a) Topographic profiles obtained with a total station showing the vertical  
 342 displacement across the studied fault at Tiberias Theatre and the Southern Gate. Each profile is  
 343 plotted on a relative vertical scale with a vertical exaggeration of ca. 4x; b-e) photos of the  
 344 measured points at Theatre (b-d) and Southern Gate (e), colored dots represent shooting points.

345 4.1.2 Archaeological evidence for damage due to shaking

346 Beside the major damage described in section 4.1.1, the investigated sites show extensive  
 347 strain features generated by transient shaking (Rodríguez-Pascua et al., 2011), such as fractures  
 348 and cracks in masonry blocks and broken corners.

349 We measured dip and dip direction of 123 fractures (in masonry blocks) in the Theatre  
 350 and 59 in the Southern Gate (Table S2). These are Mode I fractures (i.e., opening fractures),  
 351 affecting walls and building stones. Generally, they break the entire stone height, albeit in some  
 352 cases they affect a single corner of the building stone (see Fig. S14 for examples). The strike of  
 353 the fractures has a modal value of 160° and 140° in the whole Theatre and the orchestra floor,  
 354 respectively (see rose diagrams in Fig. 4a). These values are broadly consistent with the direction  
 355 of the gravity graben found within the Theatre. The distribution of fractures strike (Fig. 4a) is

356 fitting with both the orientation of the fault gouge in bedrock and with the best fit fault plane  
357 solution obtained from the inversion of the bedrock fault slip data (Fig. 4d).

358 South of the Theatre, the last excavation phase during 2017 uncovered an Umayyad water  
359 reservoir (7-8<sup>th</sup> century CE). Damage is here represented by a series of steeply inclined fractures  
360 between masonry blocks, located in a ca. 1 m wide zone (Fig. 6d). The damage zone is situated  
361 along the line connecting the graben in the Theatre and the warped Byzantine wall at the  
362 Southern Gate, i.e. on the fault line.

#### 363 4.1.3 *Terminus ante quem* for the damaging event: the Fatimid-Abassid quarter

364 The most recent building phase excavated at the Theatre site includes several buildings  
365 belonging to the Fatimid-Abassid period (8-11<sup>th</sup> century CE, Fig. 3a). Fig. 5 shows photos taken  
366 during excavations in 2009, when the Fatimid-Abassid quarter was not yet removed. In  
367 particular, Fig. 5b-d show that the damage is limited to the Roman-age flooring and to the debris  
368 flow sediments above it. The Fatimid-Abassid buildings, which lie immediately above the debris  
369 flow deposits, are never faulted nor deformed (Atrash, 2010). This observation provides a tight  
370 *terminus ante quem* for the event that damaged the Theatre, i.e., not later than the 8–11<sup>th</sup> century  
371 CE.

372 Summary of the archaeoseismic observations reveals a ~300 m long segment of the  
373 JVWB (Theatre to Gate) that ruptured the surface during an earthquake that apparently took  
374 place at the 8<sup>th</sup> century CE. Slip along the fault is normal, vertical throw is ~0.5 m.

#### 375 4.2 The Jordan Valley Western Boundary fault: geomorphology and shallow subsurface

376 To trace the JVWB further N and S of the studied archeological sites, we acquired a  
377 series of seismic lines, dug an exploratory trench across the fault trace, interpreted available  
378 borehole logs and looked for geomorphological evidence of active tectonics along-strike of the  
379 JVWB through field surveys and LiDAR interpretation. In all the three interpreted seismic lines  
380 we distinguished a Cretaceous-to-Neogene bedrock (including the Upper Cretaceous limestones  
381 and a Neogene sequence) separated from an overlying sequence of chaotic-facies unit,  
382 interpreted as Late Pleistocene loose deposits ( $V_p < 1000$  m/s), by a major unconformity. Late  
383 Pleistocene units can be attributed to different facies, including lacustrine, slope deposits and  
384 man-made reworking. The unconformity and Late Pleistocene units appear to be displaced by  
385 some of the recognized fault strands, as illustrated below.

386 The Northern seismic line (Fig. 8), 500 m long, runs ~700 m N of the Tiberias Theatre.  
387 This high-resolution reflection line images to the SW a sequence characterized by a poorly  
388 resolved chaotic facies, possibly affected by edge effects, and ca. 2200-3000 m/s  $V_p$  velocity;  
389 geological maps as well as surface outcrops allow to attribute this seismic facies to the bedrock,  
390 locally composed of Neogene clastics. A main fault zone, at depth, splays upward into a hybrid  
391 flower structure, above ca. 200 mSec TWT, including the F1 and F2 faults strands, that have  
392 been recognized also in the Line 253 (see below). Here, F2 branches out, upward, into several  
393 splays. This fault architecture, characterized by a relatively wide deformation zone, is typical of  
394 transtensive environments, consistently with the deflection of the JVWB strike and the splaying  
395 of the fault trace into several fault strands. Faults displace the unconformity and, at places, show  
396 evidence for displacing reflectors inside the Late Pleistocene deposits (e.g., F1).

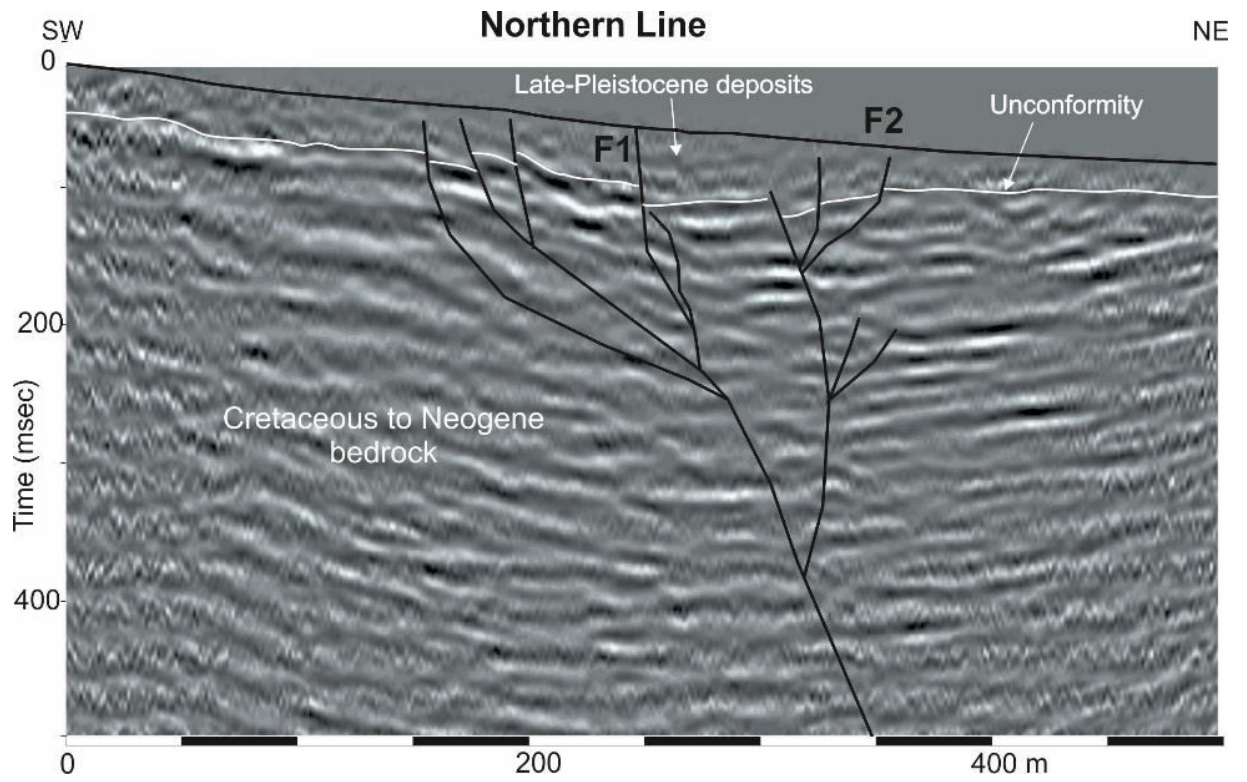
397 Line 253, 250 meters long, is located close to the Southern Gate (Fig. 9a). As was  
398 observed in the Northern line, bedrock is cut by high-angle normal faults and overlaid by chaotic

399 loose sediments. The F1 fault corresponds with a subtle topographic scarp (Fig. 2b) identified on  
400 aerial photos and that can be faintly seen in the field. F1 fault branches out, at ca. 200 mSec, into  
401 a second fault strand that show evidence of cumulative displacement and deformation of the Late  
402 Pleistocene unconformity. An exploratory trench 15 m long and 2.5 m deep was excavated along  
403 the Line 253, fully covering the projection of F1 fault on the ground surface. We aimed at  
404 digging deep enough to expose the faulted debris flow sediments of the 7<sup>th</sup>-8<sup>th</sup> century CE  
405 already encountered during the archaeological excavations at the Theatre (Figure 5e). We were  
406 not able to reach this target, because a cavity with human bones was found at the trench bottom  
407 2.5 m from the ground surface, thus preventing further excavations. However, the trench  
408 revealed reworked archeological strata throughout its entire depth. The oldest uncovered pottery  
409 artifacts can be approximately dated at the 11<sup>th</sup> century CE. No evidence for faulting was  
410 observed in the trench section (see Fig. S15). This negative evidence provides a relevant  
411 information, confirming that no surface deformation events, neither tectonic nor gravitational,  
412 occurred in the past ca. 1000 yr along F1.

413 Line 252, 700 m long, is located 2.5 km S of the Theatre (Fig. 9b), along a late  
414 Pleistocene landslide that was previously interpreted as seismically triggered (Yagoda-Biran et  
415 al., 2010; Katz et al., 2010). Here, a single fault plane, branching out upward, can be interpreted,  
416 based on the displaced Late Pleistocene unconformity and on reflectors cutoff inside the bedrock.  
417 The fault appears as overhanging in the shallowest portion and only some of the fault strands cut  
418 inside the Late Pleistocene deposits and up to the surface. At this site, we extract a 500-m long  
419 topographic profile from the LiDAR-derived DSM: the landslide toe is crossed by a 5.4-m high  
420 scarp, possibly fault-driven (Fig. S16). The westernmost fault strand appears as concealed inside  
421 the bedrock, but it is associated to a E-dipping homocline of the unconformity and associated  
422 onlap terminations in the Late Pleistocene units, above the homocline. Such a geometry could be  
423 consistent with a secondary blind fault, cutting in the footwall of the JVWB (locally in the  
424 lacustrine sediments of the Bira Fm.).

425 Further constraints on the shallow subsurface are provided by stratigraphic logs of more  
426 than 30 boreholes (see Fig. 2b) located in the immediate closeness of the study area. We pinpoint  
427 the depth of stratigraphic or lithological boundaries and used this information to constrain the 3D  
428 geometry of the layers. The typical stratigraphic column comprises, from top to bottom, i) man-  
429 made infill, ii) loose deposits including clasts, clays and basalt fragments, iii) Pleistocene  
430 lacustrine marls and iv) bedrock. Boreholes in Fig. 2b are divided in two groups according to the  
431 depth of bedrock (i.e., thickness of loose deposits). It ranges from zero where bedrock is  
432 outcropping, to over 40 m depth. The boreholes at the whole coastal area and the ones located at  
433 the outlet of wadi channels or on landslide deposits show more than 10 m of loose sediments,  
434 consistently with recent sedimentation processes. We use the few boreholes showing bedrock at  
435 depths shallower than 10 m as marking the footwall and as spatial constraints for the fault  
436 position. We have drawn three shallow geological cross-sections passing through the described  
437 sites, based on the constraints coming from the shallow boreholes, field observations and seismic  
438 reflection data (Fig. 10).

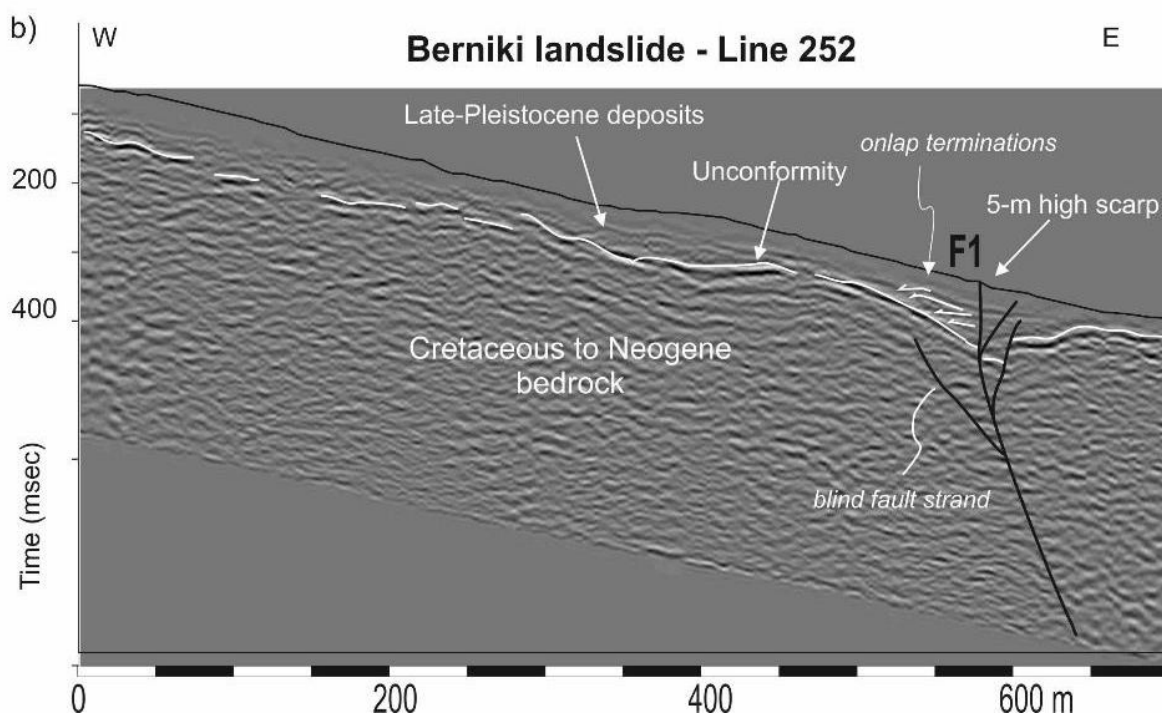
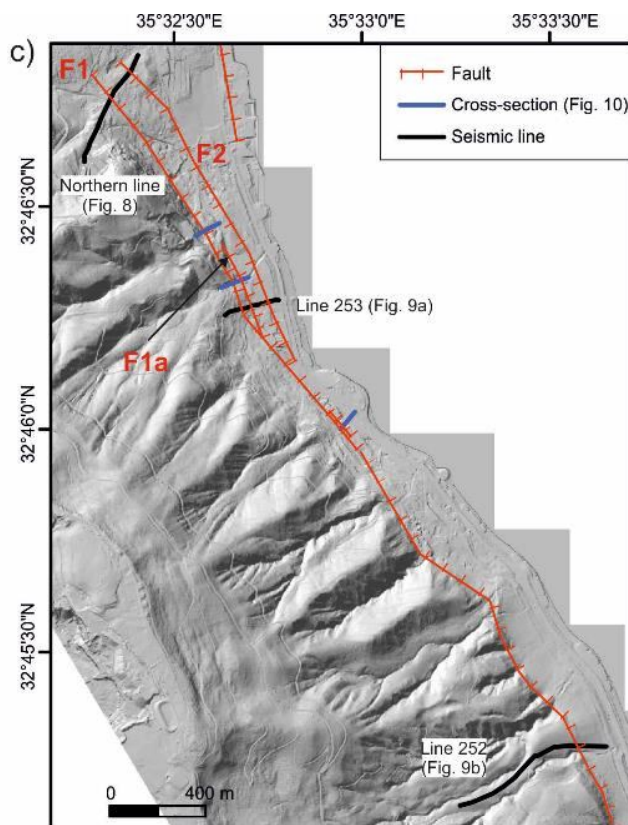
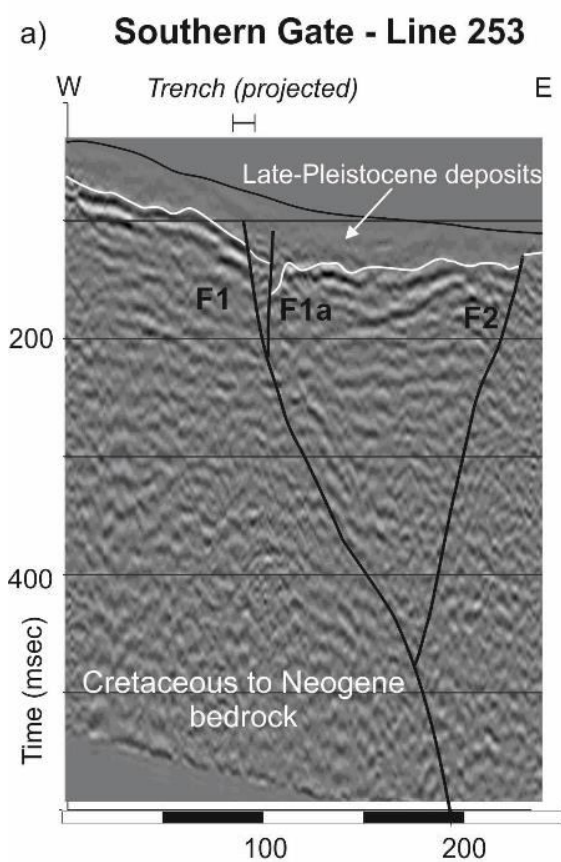
439



440  
441  
442  
443  
444

9.

**Figure 8.** Seismic line run N of Tiberias Theatre and relative interpretation; trace in Fig.



446 **Figure 9.** *Seismic lines and relative interpretation; a) Southern Gate, location of the*  
 447 *trench is also shown. b) Berniki Beach landslide. c) traces of the seismic lines.*

448

## 449 **5 Discussion and interpretations**

### 450 5.1 What generated the damage observed at Tiberias?

451 Damage of archaeological sites can be due to a number of natural or man-made events.  
 452 Ascribing that damage to a specific factor means to exclude other possible causes. In the case of  
 453 Tiberias, the following findings support coseismic surface rupture as the causative mechanism:

- 454 i) The Theatre and Southern Gate are built along the trace of a mapped fault,  
 455 manifested in the field as a contact between limestone and thin alluvial deposits.
- 456 ii) All our observations document a pure normal faulting.
- 457 iii) The gravity-graben inside the Theatre is a feature consistent with coseismic, near-  
 458 fault deformation (e.g., Slemmons, 1957; Rodriguez-Pascua et al., 2011) and is  
 459 due to the steepening of the fault plane approaching the surface.
- 460 iv) Damage is consistently found in Roman levels and in the overlaying debris flow  
 461 sediments uncovered in the Theatre, but the later Abassid levels were not faulted  
 462 nor deformed. Archaeological stratigraphy provides tight chronological  
 463 constraints, based on architectural style, building techniques and materials of the  
 464 findings and structures.

465 The lines of reasoning listed above point toward an earthquake-related damage, and more  
 466 specifically to primary surface faulting. The damaging event is constrained to later than 530 CE  
 467 and younger than the Abassid caliphate (750-1258 CE). Among the historical records of strong  
 468 earthquakes that hit the area and might have been accompanied by surface faulting, the only one  
 469 fitting with this chronological interval is the mid-8<sup>th</sup> century CE seismicity (Fig. 3).

470 The presence of a thick cover of man-made deposits, intensely reworking and altering the  
 471 natural landscape, partly justifies the difficulty in here recognizing tectonic landforms. The lack  
 472 of fault displacement since medieval times at the investigated sites suggests the absence of soil  
 473 movements due to local differential settlement, compaction, landsliding, slope processes or  
 474 aseismic creep in the closeness of the faulted archaeological sites. In fact, several strong seismic  
 475 events occurred close to Tiberias after the 8<sup>th</sup> century CE sequence, such as the 1759 and 1837  
 476 events (Ambraseys & Barazangi, 1989; Ambraseys, 1997). Severe shaking up to VIII MSK or IX  
 477 MM during these seismic events did not reactivate the mapped fault ruptures at the Theatre and  
 478 Southern Gate. This rules out a purely geotechnical and/or gravitational control on the observed  
 479 fault ruptures.

480 Moreover, comparison can be made with the strongest and most destructive earthquake  
 481 that hit the Holy Land during the past century, the 11 July 1927 Jericho earthquake. Its  
 482 magnitude was estimated by Ben-Menahem et al. (1976) to be  $M_I = 6.25$ . Recently, Avni et al.  
 483 (2002) assessed an epicentral intensity of  $MSK = IX$ . Environmental effects were numerous,  
 484 including liquefaction, landslides and slumps of the Jordan River banks, seiche and subaqueous  
 485 landslides in the Dead Sea. No surface faulting was observed, thus showing that the threshold for  
 486 extensive surface faulting along the Dead Sea and Jordan Valley is in the order of  $M_w 6.5$ .

487 Fig. 3b shows the sites where surface faulting has been related to the mid-8<sup>th</sup> century CE  
488 seismicity (see also Section 2.3). Ruptures may have been caused by a single earthquake or by a  
489 sequence of events, a topic that we address in Section 5.3.

490

## 491 5.2 Structural setting and fault displacement hazard at Tiberias

492 The reconstruction of the stratigraphic and structural setting of the shallow subsurface  
493 shows active faults displacing the ground surface; they were constrained by direct observation at  
494 the archaeological sites (Fig. 10a-b) and through the seismic lines and borehole correlation, or  
495 indirectly suggested by the existence of the hot springs (Fig. 10c).

496 Our data suggest the presence of a wider fault zone in the northern sector, where the fault  
497 branches out into several splays showing evidence for transtensional tectonics and narrowing to  
498 the south. At the Theatre the fault strand that ruptured during the earthquake sequence show  
499 evidence for a cumulative late-Pleistocene to Holocene displacement of the bedrock. At the  
500 Southern Gate the fault lies within Cretaceous limestones, as deduced from archaeoseismological  
501 observations and core drillings (Fig. 10b) whereas the late Pleistocene to Holocene cumulative  
502 displacement of bedrock is taken up by a fault splay located a few meters to the E. Seismic  
503 reflection data, however, recognized the same two fault strands as belonging to the same  
504 structure (Figs. 8 and 9).

505 Further to the south, at Berniki landslide, the described fault strands join into a single  
506 fault plane with minor branching in the shallowest part and possible evidence for blind faulting  
507 in the footwall sector, where the fault cuts through incompetent lacustrine units. The different  
508 properties of bedrock and loose sediments affect the fault pattern and expression at the surface,  
509 including the amount of displacement (Bray et al., 1994), and the distribution of displacement  
510 among different fault strands.

511 From the data above, we confirm that no evidence of strike slip faulting is detectable  
512 along the JVWB neither in the morphotectonic landscape nor in the coseismic ground rupture  
513 mapped and analyzed at ancient Tiberias and surroundings.

514 We thus support the structural interpretation that the Sea of Galilee area is structurally  
515 arranged into a partitioned system composed by the Jordan Valley Fault, to the east, and the  
516 JVWB, to the west (e.g., Garfunkel, 1981). On the Jordan Valley Fault, Holocene left-lateral and  
517 normal components are estimated to be 4 – 5 and 0.1 – 0.2 mm/yr respectively, based on both  
518 paleoseismology (Ferry et al., 2007; Katz et al., 2010) and GPS monitoring (Hamiel et al., 2016).  
519 Such a structural model implying strain partitioning along oblique margins has been documented  
520 elsewhere along the DST (Ben-Avraham and Zoback, 1992; Sagy et al., 2003; Weinberger et al.,  
521 2009) and worldwide (e.g., Lettis & Hanson, 1991; Walker et al., 2005).

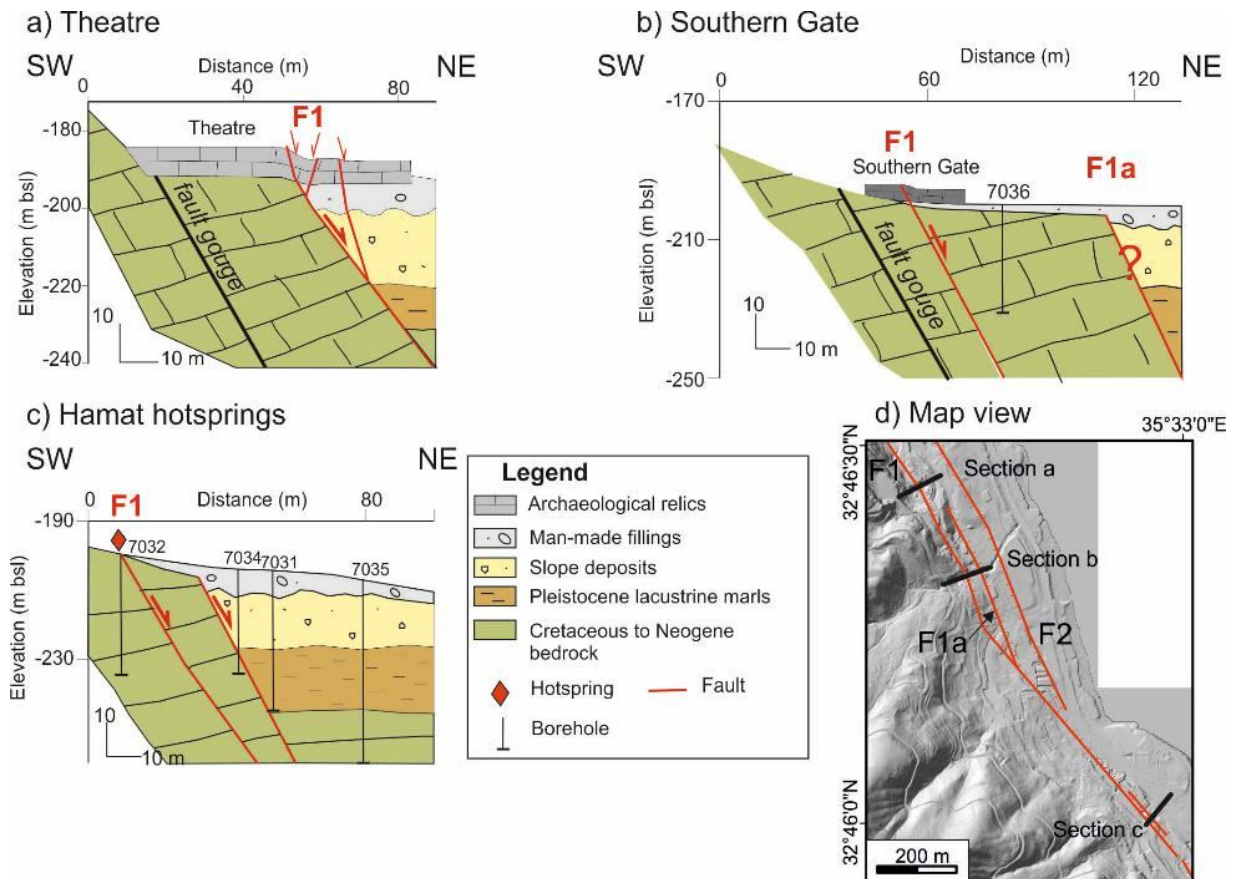


**Figure 10.** Schematic sketches of the shallow subsurface at three key positions: a) Theatre; b) Southern Gate; c) Hamat hotspots. Information on geology is derived from the Israeli geological map (Sneh, 2008), published scientific literature (e.g., Hurwitz et al., 2002) and local reports (e.g., Zaslavsky, 2009). Boreholes logs are from GSI archive; d) section traces.

### 5.3 Rupture scenarios

For better constraining the seismic hazard for the area, we consider three different rupture scenarios and calculate expected magnitude from known fault length and area adopting published scaling relations (Wells & Coppersmith, 1994; Hanks & Bakun, 2008; Wesnousky, 2008; Stirling et al., 2013). Two scenarios include the rupture of a single fault source, i.e. the Jordan Valley Western Boundary Fault (JVWB, scenario n° 1), assuming it is continuous at the subsurface as a worst-case scenario, or the Jordan Valley Fault (JVF, scenario n° 2). The third scenario accounts for the simultaneous rupture of the JVWB and JVF. Inversion of geodetic measurements as well as moderate seismicity cutoff depth indicate a locking depth of 10-15 km (Sadeh et al., 2012; Hamiel et al., 2016), close to the upper-lower crust transition (ten Brink et al., 2006), even if some works claim a deeper transition (ca. 28 km according to Garfunkel et al., 2014). The JVF and JVWB are linked above or close to the locking depth, and thus can rupture separately or together (single- or multi-fault rupture scenario *sensu* Lettis & Hanson, 1991).

For calculating the expected magnitudes, we assumed the following parameters for the faults:

- 543 - Scenario n° 1 – JVWB: normal faulting, length 45 km (Arbel to Tel Rehov and Tel  
544 Teomim; red line in Fig. 3);
- 545 - Scenario n° 2 – JVF: strike-slip faulting, length 125 km (from Beteiha to Jericho), width  
546 12.5 km (blue line in Fig. 3);
- 547 - Scenario n° 3 – JVWB and JVF: normal and strike-slip faulting, length 170 km (sum of  
548 scenario 1 and 2), width 12.5 km.

549 In the selection of the most appropriate scaling relation, we rely on the work by Stirling  
550 et al. (2013), who categorized previously published scaling relationships according to tectonic  
551 regime and style of faulting. They also assign a quality score based on the quality and quantity of  
552 the regression dataset. Following these guidelines, we select the subclass A2 which represents  
553 slow plate boundary faults (< 10 mm/yr) as the one most suitable to the rates measured along the  
554 DSF. The slip rates along the DSF are indeed constrained to 4-5 mm/yr from geological and GPS  
555 data (Garfunkel et al., 2014).

556 For the scenario n° 1 (normal faulting), we select the scaling relation published by  
557 Wesnousky (2008), which has a quality score 1 (i.e., best available) according to Stirling et al.  
558 (2013). Moment magnitude  $M_w$  is computed from surface rupture length  $L$  as:

$$559 \quad M_w = 6.12 + 0.47 \log L$$

560 Resulting in an estimated  $M_w = 6.9$  for the JVWB rupture; this finding is consistent with  
561 the 0.5 m of vertical displacement observed at the sites, which can be related to a  $M_w$  ca. 6.5  
562 event (Wells & Coppersmith, 1994).

563 For the scenarios n° 2 and 3, we select the relation by Hanks and Bakun (2008), which  
564 has a quality score 1 (i.e., best available) according to Stirling et al. (2013). For areas larger than  
565 537 square kilometers, moment magnitude  $M_w$  is computed from fault area  $A$  as:

$$566 \quad M_w = 4/3 \log A + (3.07 \pm 0.04)$$

567 Scenario n° 2 results in an estimated magnitude of 7.3, whereas scenario n° 3 results in  
568  $M_w = 7.6$ .

569 When exploring different parametrizations (i.e., fault rupture length, fault width, adopted  
570 scaling relations), we find estimated magnitudes consistent with the preferred ones (i.e.,  
571 differences of up to 0.1). Scenario n° 3 implies the coexistence of dip-slip and lateral motions, a  
572 setting that can be explained by strain partitioning.

573 Summarizing, we obtain a maximal  $M_w$  6.9 for the JVWB rupture and a  $M_w$  7.3 for the  
574 JVF. The multi-fault scenario results in a  $M_w$  7.6 earthquake. Our magnitude estimates are  
575 consistent with those suggested in the literature (i.e.,  $M_s$  7.0 – 7.5; Marco et al., 2003; Hamiel et  
576 al., 2009; Zohar et al., 2016), but we underline that our calculations represent worst-case  
577 scenarios, in which the earthquake ruptures the entire fault. Complete fault ruptures may be  
578 obstructed by structural thresholds; we highlight the presence of a prominent fault bend in the  
579 JVWB fault trace just N of Tiberias, and we maintain that partial fault ruptures may occur as  
580 well, resulting in smaller magnitudes. For example, Marco et al. (2003) proposed that normal  
581 faulting at Tiberias represent the NW-striking termination of a strike-slip rupture along the JVF,  
582 where sinistral strike-slip is transformed to normal slip. The simultaneous rupture of JVWB and  
583 JVF for their entire lengths (Scenario n° 3) is considered unlikely, but such occurrence should  
584 not be discarded in seismic hazard evaluations.

585 Other events may have occurred in the mid-8<sup>th</sup> century CE more to the N (Yammounch  
586 and/or Missyaf Faults) or S of the Dead Sea, but their evaluation is beyond the scope of the  
587 present paper.

588 The occurrence of multiple shocks in a short time interval is a common pattern in the  
589 DSF region, as clearly documented in the historical record (e.g., Karcz, 2004; Ambraseys, 2005,  
590 2009) and by geological studies (Agnon, 2014; Marco and Klinger, 2014; Lefevre et al., 2018).  
591 The present study documents an additional fault with evidence of surface ruptures within a  
592 region with already known major active faults. This finding, coupled with earthquake clustering,  
593 will help to better depict the seismic landscape (Michetti et al., 2005) in the Sea of Galilee  
594 region.

595

## 596 **6 Conclusions**

597 The geometry, kinematics and activity of the faults crossing the town of Tiberias, studied  
598 through an integrated structural, archaeoseismological and geophysical approach revealed that  
599 this segment was activated in the mid-8<sup>th</sup> century CE.

600 We propose that normal motion on the W side of the Sea of Galilee can coexist with  
601 strike-slip motion in the E side, in a strain-partitioned model. Based on the results of this study,  
602 we suggest that multi-fault rupture may be more frequent than the occurrence of single-fault  
603 ruptures in the Sea of Galilee region. This must be considered in any seismic hazard evaluation  
604 for this area. The absence of instrumental measurements of strong ( $M_w$  greater than 6.0)  
605 earthquakes with normal fault focal mechanism should not be construed as evidence that similar  
606 events will never occur along this section of the Dead Sea Fault.

607 Our research provides useful inputs for developing updated building codes in the region:  
608 measures to reduce exposure and the overall seismic risk (e.g., avoidance zones, setback  
609 distances) must rely on the unequivocal definition of active fault traces and their  
610 characterization. Normal faulting is not adequately addressed in the current tectonic models and  
611 seismic hazard assessment in the Sea of Galilee; instead, our results point out that, beside strike-  
612 slip motion, normal faulting must be considered as well. We argue that the renewed attention of  
613 the public opinion, driven by the recent seismicity, can be an incentive to act on mitigation and  
614 preparedness measures.

615

## 616 **Acknowledgments**

617 We wish to thank Tiberias Municipality, the Israel Antiquity Authority, the Geophysical Institute  
618 of Israel, Y. Nahmias (GSI), E. Hassul and Y. Darvasi (Neev Center for Geoinformatics at the  
619 Hebrew University). We are grateful to S. Marco for kindly handing us the pictures of the  
620 Theatre excavations in 2009; to the Associate Editor F. Rossetti and to A. Agnon, S. Marco, Z.  
621 Mildon and two anonymous reviewers for thoughtful comments. Fondazione Banca del Monte di  
622 Lombardia fellowship allowed a 6-months stay of MFF at GSI. The work was supported by the  
623 Israeli National Steering Committee for Earthquake Preparedness. Historical seismicity is from  
624 <http://seis.gii.co.il/en/earthquake/searchEQSRslt.php>, the reports on archaeological excavations  
625 are from [http://www.hadashot-esi.org.il/default\\_eng.aspx](http://www.hadashot-esi.org.il/default_eng.aspx) (last accessed February 2020). Other  
626 data are available from the listed references.

627

628 **References**

- 629 Agnon, A., (2014). Pre-Instrumental Earthquakes Along the Dead Sea Rift. In Dead Sea  
630 Transform Fault System: Reviews, 207-261.
- 631 Alfonsi, L., Cinti, F.R., & Ventura, G. (2013). The Kinematics of the 1033 AD Earthquake  
632 Revealed by the Damage at Hisham Palace (Jordan Valley, Dead Sea Transform Zone).  
633 *Seism. Res. Lett.*, 84(6), 997-1003.
- 634 Allmendinger, R.W., Marrett, R.A., & Cladouhos, T.T. (2001). FaultKinWin: a program for  
635 analyzing fault slip data for Windows™ computers.  
636 <http://www.geo.cornell.edu/geology/faculty/RWA/programs/>
- 637 Ambraseys, N. (1997). The earthquake of 1 January 1837 in Southern Lebanon and Northern  
638 Israel. *Ann. Geofis.* XL (4), 923–935.
- 639 Ambraseys, N. N. (2005). The seismic activity in Syria and Palestine during the middle of the  
640 8th century; an amalgamation of historical earthquakes. *J of Seism*, 9(1), 115-125.
- 641 Ambraseys, N. (2009). Earthquakes in the Mediterranean and Middle East: a multidisciplinary  
642 study of seismicity up to 1900: Cambridge University Press.
- 643 Ambraseys, N., & Barazangi, M. (1989). The 1759 Earthquake in the Bekaa valley: implications  
644 for earthquake hazard assessment in Eastern Mediterranean region. *J. Geophys. Res.* 94,  
645 4007–4013.
- 646 Atrash, W. (2010). Tiberias, the Roman Theater. [http://www.hadashot-](http://www.hadashot-esi.org.il/report_detail_eng.aspx?id=1381&mag_id=117)  
647 [esi.org.il/report\\_detail\\_eng.aspx?id=1381&mag\\_id=117](http://www.hadashot-esi.org.il/report_detail_eng.aspx?id=1381&mag_id=117)
- 648 Avni, R., Bowman, D., Shapira, A., & Nur, A. (2002). Erroneous interpretation of historical  
649 documents related to the epicenter of the 1927 Jericho earthquake in the Holy Land.  
650 *Journal of seismology*, 6(4), 469-476.
- 651 Ben-Avraham, Z., & Zoback, M. (1992). Transform-normal extension and asymmetric basins: an  
652 alternative to pull-apart models. *Geology*, 20, 423-426.
- 653 Ben-Menahem A., Nur, A. & Vered, M. (1976). Tectonics, seismicity and structure of the Afro-  
654 Eurasian junction-the breaking of the incoherent plate. *Phys. Earth Planet Interiors* 12, 1–  
655 50. Bogoch, R., & Sneh, A. (2008). Geological map of Israel, 1:50,000, Sheet 4-I Arbel.  
656 GSI, Jerusalem.
- 657 Bozorgnia, Y., & Bertero, V. V. (2004). Earthquake engineering: from engineering seismology  
658 to performance-based engineering. CRC press.
- 659 Bray, J. D., Seed, R. B., Cluff, L. S., & Seed, H. B. (1994). Earthquake fault rupture propagation  
660 through soil. *Journal of Geotechnical Engineering*, 120(3), 543-561.
- 661 Dalali-Amos, E. (2016). Excavations at Tiberias, Final report, Hadashot Arkheologiyot, 128  
662 [http://hadashot-esi.org.il/report\\_detail\\_eng.aspx?id=25056&mag\\_id=124](http://hadashot-esi.org.il/report_detail_eng.aspx?id=25056&mag_id=124)
- 663 Daëron, M., Klinger, Y., Tapponnier, P., Elias, A., Jacques, E., & Sursock, A. (2007). 12,000-  
664 year-long record of 10 to 13 paleoearthquakes on the Yammouneh fault, Levant fault  
665 system, Lebanon. *Bulletin of the Seismological Society of America*, 97(3), 749-771.

- 666 Eppelbaum, L., Ben-Avraham, Z., Katz, Y., & Marco, S. (2004). Sea of Galilee: comprehensive  
667 analysis of magnetic anomalies: *Isr. J. Earth Sci.*, 53, p. 151–171.
- 668 Eppelbaum, L.V., Ben-Avraham, Z., & Katz, Y. (2007). Structure of the Sea of Galilee and  
669 Kinarot Valley derived from combined geological geophysical analysis. *First break*,  
670 25(1), 43-50.
- 671 Ferry, M., Meghraoui, M., Abou Karaki, N., Al-Taj, M., Amoush, H., Al-Dhaisat, S., & Barjous,  
672 M. (2007). A 48-kyr-long slip rate history for the Jordan Valley segment of the Dead Sea  
673 fault. *EPSL* 260, 394–406.
- 674 Garfunkel, Z. (1981). Internal structure of the Dead Sea leaky transform (rift) in relation to plate  
675 kinematics. *Tectonophysics* 80, 81–108.
- 676 Garfunkel, Z., Zak, I., & Freund, R. (1981). Active faulting in the Dead Sea rift. *Tectonophysics*,  
677 80(1-4), 1-26.
- 678 Garfunkel, Z., Ben-Avraham, Z., & Kagan, E. (Eds.) (2014). *Dead Sea transform fault system:*  
679 *reviews*. Vol. 6, Springer.
- 680 Guidoboni, E., Ferrari, G., Mariotti, D., Comastri, A., Tarabusi, G., & Valensise, G. (2007).  
681 Catalogue of Strong Earthquakes in Italy (461 BC-1997) and Mediterranean Area (760  
682 BC-1500).
- 683 Hamiel, Y., Amit, R., Begin, Z. B., Marco, S., Katz, O., Salamon, A., Zilberman, E., & Porat, N.  
684 (2009). The seismicity along the Dead Sea Fault during the last 60,000 years. *Bulletin of*  
685 *the Seismological Society of America*, 99(3), 2020-2026.
- 686 Hamiel, Y., Piatibratova, O., & Mizrahi, Y. (2016). Creep along the northern Jordan Valley  
687 section of the Dead Sea Fault. *Geophys Res Lett*, 43.
- 688 Hanks, T. C., & Bakun, W. H. (2008).  $M - \log A$  observations of recent large earthquakes. *Bull.*  
689 *Seismol. Soc. Am.*, 98(1), 490–494.
- 690 Hartal, M., Dalali-Amos, E., & Hilman, A. (2010). Preliminary report on the excavations at  
691 Tiberias. [http://hadashot-esi.org.il/report\\_detail\\_eng.aspx?id=1574&mag\\_id=117](http://hadashot-esi.org.il/report_detail_eng.aspx?id=1574&mag_id=117)
- 692 Hazan, N., Stein, M., Agnon, A., Marco, S., Nadel, D., Negendank, F.W., et al. (2005). The late  
693 Quaternary limnological history of Lake Kinneret (Sea of Galilee). *Israel Quat Res* 63,  
694 60–77.
- 695 Hirschfeld, Y., & Meir, E. (2004). Tiberias, Hadashot Arkheologiyot, 118,  
696 [http://www.hadashot-esi.org.il/report\\_detail\\_eng.aspx?id=337&mag\\_id=111](http://www.hadashot-esi.org.il/report_detail_eng.aspx?id=337&mag_id=111)
- 697 Hirschfeld, Y., & Gutfeld, O. (2008). Tiberias. Excavations in the House of the Bronzes. Final  
698 Report, Volume I. Qedem Monographs of the Institute of Archaeology.
- 699 Hurwitz, S., Garfunkel, Z., Ben-Gai, Y., Reznikov, M., Rotstein, Y., & Gvirtzman, H. (2002).  
700 The tectonic framework of a complex pull-apart basin: seismic reflection observations in  
701 the Sea of Galilee, Dead Sea transform. *Tectonophysics*, 359(3), 289-306.
- 702 Ilani, S., Minster, T., Kronfeld, J., & Even, O. (2006). The source of anomalous radioactivity in  
703 the springs bordering the Sea of Galilee. *Israel, J of env radioactivity*, 85(1), 137-146.
- 704 Karcz, I. (2004). Implications of some early Jewish sources for estimates of earthquake hazard in  
705 the Holy Land. *Ann of Geoph*, 47(2-3).

- 706 Katz, O., Amit, R., Yagoda-Biran, G., Hatzor, Y., Porat, N., & Medvedev, B. (2010). Quaternary  
 707 earthquakes and landslides in the Sea of Galilee area, the Dead Sea Transform;  
 708 paleoseismic analysis and evaluation of current hazard. *Isr J Earth Sci*, 58: 275-294.
- 709 Lefevre, M., Klinger, Y., Al-Qaryouti, M., Le Béon, M., & Moumani, K. (2018). Slip deficit and  
 710 temporal clustering along the Dead Sea fault from paleoseismological investigations.  
 711 *Scientific reports*, 8(1), p.4511.
- 712 Lettis, W.R., & Hanson, K.L. (1991). Crustal strain partitioning: Implications for seismic-hazard  
 713 assessment in western California. *Geology*, 19(6), 559-562.
- 714 Makovsky, Y., Wunch, A., Ariely, R., Shaked, Y., Rivlin, A., Shemesh, A., Avraham, Z.B., &  
 715 Agnon, A. (2008). Quaternary transform kinematics constrained by sequence stratigraphy  
 716 and submerged coastline features: The Gulf of Aqaba. *Earth and Planetary Science*  
 717 *Letters*, 271(1-4), 109-122.
- 718 Marco, S. (2008). Recognition of earthquake-related damage in archaeological sites: Examples  
 719 from the Dead Sea fault zone: *Tectonophysics*, v. 453, doi:10.1016/j.tecto.2007.04.011.
- 720 Marco, S., & Klinger, Y. (2014). Review of On-Fault Palaeoseismic Studies Along the Dead Sea  
 721 Fault. In *Dead Sea Transform Fault System: Reviews*, 183-205.
- 722 Marco, S., Hartal, M., Hazan, N., Lev, L., & Stein, M. (2003). Archaeology, history, and geology  
 723 of the A.D. 749 earthquake, Dead Sea Transform. *Geology*, 31 (8) 665-668.
- 724 Marco, S., Rockwell, T.K., Heimann, A., Frieslander, U., & Agnon, A. (2005). Late Holocene  
 725 activity of the Dead Sea Transform revealed in 3D palaeoseismic trenches on the Jordan  
 726 Gorge segment. *Earth and Planetary Science Letters* 234 (2005) 189– 205.
- 727 Marrett, R., & Allmendinger, R.W. (1990). Kinematic analysis of fault-slip data. *Journal of*  
 728 *Structural Geology* 12(8), 973–986.
- 729 Medvedev, B. (2008). Faults mapping in Berniki area, Western Sea of Galilee, The Geophysical  
 730 Institute of Israel, report: 645/319/08 (in Hebrew).  
 731 <http://mapi.gov.il/earthquake/documents/j.pdf>
- 732 Meghraoui, M., Gomez, F., Sbeinati, R., Van der Woerd, J., Mouty, M., Darkal, A. N., et al.  
 733 (2003). Evidence for 830 years of seismic quiescence from palaeoseismology,  
 734 archaeoseismology and historical seismicity along the Dead Sea fault in Syria. *Earth and*  
 735 *Planetary Science Letters*, 210(1-2), 35-52.
- 736 Michetti, A. M., Audemard F. A., & Marco, S. (2005). Future trends in paleoseismology:  
 737 Integrated study of the seismic landscape as a vital tool in seismic hazard analyses.  
 738 *Tectonophysics*, 408(1-4), 3-21.
- 739 Onn, A., & Weksler-Bdolah, S. (2016). Tiberias, Gane Hammat, Hadashot Arkheologiyot 128  
 740 [http://www.hadashot-esi.org.il/Report\\_Detail\\_Eng.aspx?id=25097](http://www.hadashot-esi.org.il/Report_Detail_Eng.aspx?id=25097)
- 741 Reches, Z., & Hoexter, D.F. (1981). Holocene seismic and tectonic activity in the Dead Sea area.  
 742 *Tectonophysics* 80:235–254.
- 743 Rodriguez-Pascua, M. A., Pérez-López, R., Giner-Robles, J.L., Silva, P.G., Garduño-Monroy,  
 744 V.H., & Reicherter, K. (2011). A comprehensive classification of Earthquake

- 745 Archaeological Effects (EAE) in archaeoseismology: Application to ancient remains of  
746 Roman and Mesoamerican cultures. *Quat Int* 242(1), 20-30.
- 747 Rotstein, Y., Bartov, Y., & Frieslander, U. (1992). Evidence for local shifting of the main fault  
748 and changes in the structural setting, Kinarot basin, Dead Sea transform. *Geology*, 20(3),  
749 251-254.
- 750 Sadeh, M., Hamiel, Y., Ziv, A., Bock, Y., Fang, P., & Wdowinski, S. (2012). Crustal  
751 deformation along the Dead Sea Transform and the Carmel Fault inferred from 12 years  
752 of GPS measurements. *Journal of Geophysical Research*, 117, 1-14.
- 753 Sagy, A., Reches, Z.E., & Agnon, A. (2003). Hierarchic three-dimensional structure and slip  
754 partitioning in the western Dead Sea pull-apart. *Tectonics*, 22(1).
- 755 Sagy, A., Sneh, A., Rosensaft, M., & Bartov, Y. (2016). Map of active faults and potentially  
756 active faults for the Israel Standard 413 “design provisions for earthquakes resistance of  
757 structures”, Update 2016.  
758 [http://www.gsi.gov.il/uploads/ftp/Active\\_Faults\\_maps/2016\\_map\\_English.pdf](http://www.gsi.gov.il/uploads/ftp/Active_Faults_maps/2016_map_English.pdf)
- 759 Slemmons, D. B. (1957). Geological effects of the Dixie Valley – Fairview Peak, Nevada,  
760 earthquakes of December 16, 1954. *Bulletin of the Seismological Society of America*,  
761 47(4), 353-375.
- 762 Sharon, M., Sagy, A., Kurzon, I., Marco, S., Ben-Avraham, Z., & Rosensaft, M. (2018).  
763 Quaternary fault map of Israel. Jerusalem, 2018  
764 [http://www.gsi.gov.il/uploads/ftp/GeologicalMap/Quaternary\\_fault\\_Map\\_Israel.pdf](http://www.gsi.gov.il/uploads/ftp/GeologicalMap/Quaternary_fault_Map_Israel.pdf)
- 765 Sharon, M., Sagy, A., Kurzon, I., Marco, S., & Rosensaft M. (2020). Assessment of seismic  
766 sources and capable faults through hierarchic tectonic criteria: implications for seismic  
767 hazard in the Levant. *Natural Hazards and Earth System Sciences*, 20(1), 125-148,  
768 <https://doi.org/10.5194/nhess-20-125-2020>.
- 769 Sneh, A. (2008). Geological map of Israel, 1:50,000, Sheet 4-II Teverya: GSI, Jerusalem.  
770 <http://www.gsi.gov.il/eng/?CategoryID=253&ArticleID=763>
- 771 Sneh, A., & Weinberger, R. (2014). Major geological structures of Israel and environs, scale  
772 1:500.000, Geological Survey of Israel.  
773 <http://www.gsi.gov.il/eng/?CategoryID=298&ArticleID=751>
- 774 Stirling, M., Goned, T., Berryman, K., & Litchfield, N. (2013). Selection of Earthquake Scaling  
775 Relationships for Seismic-Hazard Analysis. *Bull. Seismol. Soc. Am.*, 103(6), 1-19.
- 776 Ten Brink, U., Rybakov, M., Al Zoubi, A.S., Hassouneh, M., Frieslander, U., Batayneh, A.T., et  
777 al. (1999). Anatomy of the Dead Sea transform: Does it reflect continuous changes in  
778 plate motion?. *Geology*, 27(10), 887-890.
- 779 Ten Brink, U., Al-Zoubi, A., Flores, C.H., Rotstein, Y., Qabbani, I., Harder, S.H. & Keller, G.R.,  
780 (2006). Seismic imaging of deep low-velocity zone beneath the Dead Sea basin and  
781 transform fault: Implications for strain localization and crustal rigidity. *Geophysical*  
782 *Research Letters*, 33(24).
- 783 Tsafir, Y., & Foerster, G. (1992). The dating of the “Earthquake of the Sabbatical year” of 749  
784 CE in Palestine. *Bull of the School of Oriental and African Studies, Univ of London*,  
785 55(2), 231-235.

- 786 Vered, M., & Striem, H. L. (1977). A macroseismic study and the implications of structural  
787 damage of two recent major earthquakes in the Jordan Rift. *Bulletin of the Seismological*  
788 *Society of America*, 67(6), 1607-1613. Walker, J. D., Kirby, E., & Andrew, J.E. (2005).  
789 Strain transfer and partitioning between the Panamint Valley, Searles Valley, and Ash  
790 Hill fault zones, California. *Geosphere*, 1(3), 111-118.
- 791 Wechsler, N., Rockwell, T.K., & Klinger, Y. (2018). Variable slip-rate and slip-per-event on a  
792 plate boundary fault: The Dead Sea fault in northern Israel. *Tectonophysics*, 722, 210-  
793 226.
- 794 Weinberger, R., Gross, M. R., & Sneh, A. (2009). Evolving deformation along a transform plate  
795 boundary: example from the Dead Sea Fault in northern Israel. *Tectonics*, 28(5).
- 796 Wells, D. L., & Coppersmith, K. J. (1994). New empirical relationships among magnitude,  
797 rupture length, rupture width, rupture area, and surface displacement. *Bulletin of the*  
798 *seismological Society of America*, 84(4), 974-1002.
- 799 Wesnousky, S.G. (2008). Displacement and geometrical characteristics of earthquake surface  
800 ruptures: Issues and implications for seismic hazard analysis and the process of  
801 earthquake rupture. *Bull. Seismol. Soc. Am.*, 98(4), 1609–1632.
- 802 Wetzler, N., Shalev, E., Göbel, T., Amelung, F., Kurzon, I., Lyakhovskiy, V., & Brodsky, E. E.  
803 (2019). Earthquake swarms triggered by groundwater extraction near the Dead Sea Fault.  
804 *Geophysical Research Letters*, 46, 8056–8063. <https://doi.org/10.1029/2019GL083491>
- 805 Yagoda-Biran, G., Hatzor, Y.H., Amit, R., & Katz, O., (2010). Constraining regional paleo peak  
806 ground acceleration from back analysis of prehistoric landslides: example from Sea of  
807 Galilee, Dead Sea transform. *Tectonophysics* 490, 81-91.
- 808 Zaslavsky, Y. (2009). Site effect and seismic hazard microzonation across the town of Tiberias,  
809 GSI Report No 502/416/09. <http://mapi.gov.il/earthquake/documents/tiberias-09.pdf>
- 810 Zilbermann, E., Amit, R., Bruner, I., & Nahmias, Y. (2004). Neotectonic and paleoseismic study  
811 – Bet She'an Valley: Report GSI/15/04  
812 [http://www.gsi.gov.il/Eng/Uploads/52bet\\_shean\\_paleo.pdf](http://www.gsi.gov.il/Eng/Uploads/52bet_shean_paleo.pdf)
- 813 Zingboym O. & Hartal, M. (2011). Tiberias, preliminary report, Hadashot Arkheologiyot 123  
814 [http://hadashotesi.org.il/report\\_detail\\_eng.aspx?id=1821&mag\\_id=118](http://hadashotesi.org.il/report_detail_eng.aspx?id=1821&mag_id=118)
- 815 Zohar, M., Salamon, A., & Rubin, R. (2016). Reappraised list of historical earthquakes that  
816 affected Israel and its close surroundings. *J Seismol*, 20(3), 971-985.
- 817 Zohar, M. (2019). Temporal and Spatial Patterns of Seismic Activity Associated with the Dead  
818 Sea Transform (DST) during the Past 3000 Yr. *Seism. Res. Lett.*, doi:  
819 10.1785/0220190124.